Astrophysical Observations of a Dark Matter-Baryon Fifth Force

Moira I. Gresham,¹ Vincent S. H. Lee,² and Kathryn Zurek²

¹ Whitman College, Walla Walla, WA

² Walter Burke Institute for Theoretical Physics,

California Institute of Technology, Pasadena, CA

Abstract

We consider the effects of an attractive, long-range Yukawa interaction between baryons and dark matter (DM), focusing in particular on temperature and pulsar timing observations of neutron stars (NSs). We show that such a fifth force, with strength modestly stronger than gravity at ranges greater than tens of kilometers (corresponding to mediator masses less than 10^{-11}eV), can dramatically enhance dark matter kinetic heating, capture, and pulsar timing Doppler shifts relative to gravity plus short range interactions alone. Using the coldest observed NS and pulsar timing array (PTA) data, we derive limits on fifth force strength over a DM mass range spanning light dark matter up to order solar mass composite DM objects. We also consider an indirect limit by combining bullet cluster limits on the DM self-interaction with weak equivalence principle test limits on baryonic self-interactions. We find the combined indirect limits are moderately stronger than kinetic heating and PTA limits, except when considering a DM subcomponent.

CONTENTS

| I. | Introduction | 3 |
|------|---|----|
| II. | Limits from NS Temperature Observations | 4 |
| | A. Grazing heating rate | 7 |
| | 1. $\Delta E_{\rm graze}$ | 7 |
| | $2.~\dot{N}_{ m graze}$ | 9 |
| | B. Captured heating rate | 10 |
| | 1. $\Delta E_{\rm cap}$ | 10 |
| | $2.~\dot{N}_{ m cap}$ | 11 |
| | C. Capture assisted by short-range interactions | 11 |
| | D. Cooling timescale and continuous heating approximation | 12 |
| | E. Limits | 13 |
| III. | Limits from Pulsar Timing Arrays | 18 |
| IV. | Inferred Limits from Equivalence Principle Tests and the Bullet Cluster | 21 |
| | A. Weak Equivalence Principle Tests | 22 |
| | B. Bullet Cluster limit | 24 |
| V. | Summary and Conclusions | 25 |
| | Acknowledgments | 27 |
| Α. | Classical Orbits and $b_{ m max}$ | 27 |
| В. | Timescale for heating once captured | 31 |
| С. | Pulsar Glitches | 33 |
| | References | 34 |

I. INTRODUCTION

A long-range fifth force between baryonic matter has long been the focus of both theoretical and experimental inquiry, as reviewed in Ref. [1]. If DM also interacts with baryons via an attractive fifth force, it induces a potential,

$$V_{\text{Yuk}}(r) = -\tilde{\alpha} \frac{GMm_X}{r} e^{-r/\lambda},\tag{1}$$

where m_X and M are the masses of the DM and a macroscopic baryonic object, respectively, when the sizes of both objects are much smaller than the force range, λ , and separation, r. This potential can arise from an effective interaction $\mathcal{L} \supset g_X \phi \bar{X} X + g_n \phi \bar{n} n$ where X and nare the effective DM and nucleon fields, and ϕ can be either a massive but very light scalar or vector field. The effective coupling in this simplified model is

$$\tilde{\alpha} \approx \frac{g_n g_X}{4\pi G m_n m_X},\tag{2}$$

where the approximation holds well when the fifth force and gravitational binding energies are subdominant contributors to the mass, M. Here we have in mind that m_X could be the mass of a macroscopic DM object such as a nugget of asymmetric DM [2–9].

The goal of this paper is to consider the astrophysical observables of such a DM-baryon fifth force ¹, focusing on a few simple tests that constrain such an interaction. Focusing on astrophysical tests implies that we are interested in force ranges $20 \,\mathrm{km} \ll \lambda \ll \mathrm{kpc}$, corresponding to (ultralight) mediator masses $10^{-11} \,\mathrm{eV} \gg m_\phi \gg 10^{-26} \,\mathrm{eV}$. Firstly, one must consider the constraints separately on g_n and g_X , which are dominated by the MICROSOPE mission's weak equivalence principle (WEP) test [11, 12] and DM self-interactions [13–15], respectively. Combining these constraints allows one to derive a bound on $\tilde{\alpha}$, shown in Fig. 1 as "bullet cluster + WEP" for two different astrophysical force ranges. Note, importantly, that this combination of bounds will lift quickly for a DM sub-component, only weakly constrained by observations of DM halos.

The majority of this paper will focus on a pair of constraints that weaken only linearly with the DM density for a DM sub-component. These come from heating of neutron stars (NSs) from DM capture, and pulsar timing measurements of transiting DM clumps, where

¹ A recent work on long-range DM-baryon fifth force with a different set-up can be found in [10].

² Above the kpc scale, torsion balance tests of differential accelerations toward the galactic center limit the baryon-DM force to be weaker than gravity. The lower limit is set by neutron star diameters.

DM passing near pulsars enhance the Doppler effect on the pulsar frequencies [16–27]. These two constraints on the DM-baryon fifth force, which we derive in detail below, are summarized in Fig. 1, labeled as "heating" and "PTA." The heating constraints are further shown for two different limits: first, where the DM interactions beyond gravity are only via the fifth force (labeled as "tidal"), and, second, where the DM has not only the fifth force to focus it onto the NS but also a short range interaction to capture it with high efficiency (labeled as "maximal").

Heating of NSs via DM capture has been considered previously for the case of a short-range interaction, such as for WIMPs and hidden sector DM [28–47]. However, when the force range is longer than a typical NS diameter, $\lambda > 20 \,\mathrm{km}$ ($m_{\phi} < 10^{-11} \,\mathrm{eV}$), a DM-baryon force accelerates and focusses DM more than through gravity alone, leading to observable effects via two different mechanisms which we compute in detail. First, more DM is focussed on the NS due to the fifth force. Second, the DM is more energetic when it arrives at the NS surface, which we show then dominantly heats the NS via seismic oscillations. We then extract the heating constraints utilizing the coldest observed NS (PSR J2144-3933, from Hubble Space Telescope) by requiring that the kinetic energy of all the captured DM raise the temperature by an amount less than the observed (unredshifted surface) temperature, $T_s < 42,000 \,\mathrm{K}$ [48].

The rest of the paper is devoted to deriving in detail the constraints on the DM-baryon fifth force coupling $\tilde{\alpha}$ outlined in Fig. 1. In Sec. II, we derive the kinetic heating rate and resulting NS luminosity in the presence of a fifth force interaction. Some of the details are relegated to Appendices. In Sec. III, we outline the procedure for deriving fifth force constraints with PTA observations, and show the results using the 11-year dataset [49, 50] by NANOGrav [51]. In Sec. IV, we consider observations from WEP tests and the bullet cluster, and derive indirect upper limits on the DM-baryon interaction. Finally, in Sec. V, we conclude.

II. LIMITS FROM NS TEMPERATURE OBSERVATIONS

Transiting DM can heat NSs to higher-than-expected temperatures observable by the next generation of infrared telescopes, including the James Webb Space Telescope (JWST) [28]. As discussed in [28], if the energy deposited by DM passing near a NS is dissipated through

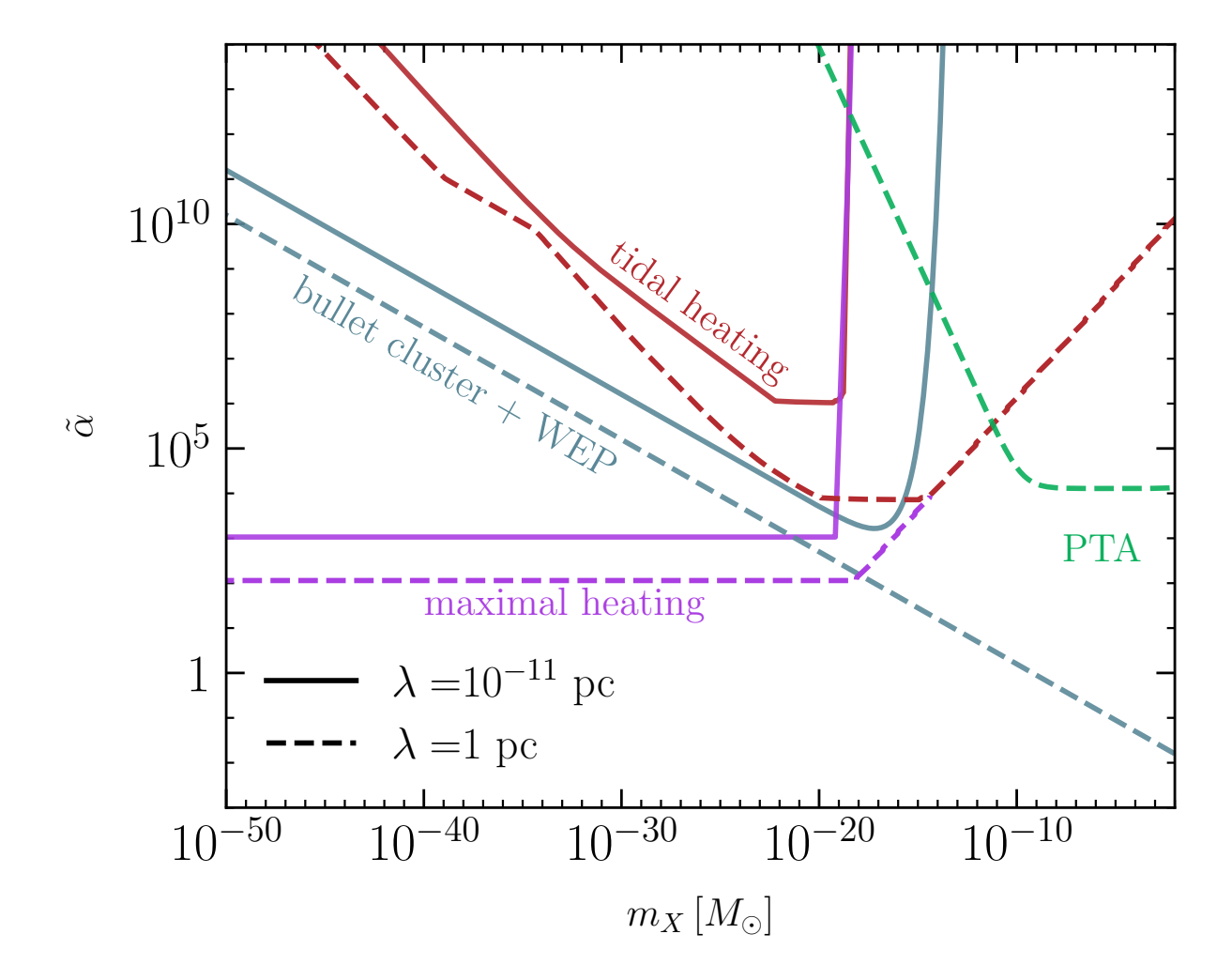


FIG. 1. Summary of the bounds derived in this paper on the DM-baryon fifth force to gravitational force strength ratio, $\tilde{\alpha}$, as defined in Eq. 1, for force ranges, λ , at the two extremes of the range we consider. The relevant equations for tidal heating, maximal heating, PTA, and bullet cluster + WEP are derived in Sec. II A-II B, Sec. II C, Sec. III, and Sec. IV B respectively.

black-body radiation, then in the local rest frame of the NS, the thermal photon luminosity due to dark kinetic heating is $L_{\gamma}^{\rm DM} = \dot{E}_{\rm kin}$. Given an unredshifted surface temperature measurement $T_{\rm s,i} \leq T_{\rm s,i_{max}}^{\rm meas}$ for a particular NS, i, with radius, R, we can infer a limit on the factors contributing to $\dot{E}_{\rm kin}$ through³

$$\dot{E}_{\rm kin} < \sigma_{\rm B} 4\pi R^2 \left(T_{\rm s,i_{\rm max}}^{\rm meas} \right)^4, \tag{3}$$

³ Redshifted surface temperature, T^{∞} , is related to unredshifted temperature, T, through $T = \frac{T^{\infty}}{\sqrt{1 - \frac{2GM}{R}}}$.

where the heating rate is schematically given by

$$\dot{E}_{\rm kin} \approx \dot{N} \Delta E,$$
 (4)

with \dot{N} and ΔE being the relevant DM flux and single-DM energy transfer, respectively.

All previous analyses of DM kinetic heating of NSs have focused on short-range DM interactions. As explained in [28], in this case, DM can deposit energy on a NS only if it intersects the NS, requiring impact parameters less than $b_{\rm max}^{\rm grav} = v^{-1} \sqrt{2GMR/(1-2GM/R)}$. At a maximum, an order one fraction of DM that intersects the NS is captured and deposits all of its kinetic energy at the NS surface, also known as the gravitational binding energy released in the capture process. Hence $\Delta E_{\rm max}^{\rm grav} \approx GMm_X/R$ and $\dot{N}_{\rm max}^{\rm grav} \approx (\rho_X/m_X)\pi \langle b_{\rm max}^2 v \rangle$, leading to a maximum heating rate from DM focused by gravity onto typical NSs near our galactic radius $(GM/R \sim 0.2, \langle v \rangle \sim 10^{-3}, \, \rho_X \sim 0.4 \, {\rm GeV/\,cm^3})$,

$$\dot{E}_{\rm kin, \, max}^{\rm grav} \approx \frac{GMm_X}{R} \pi \frac{\rho_X}{m_X} \langle (b_{\rm max}^{\rm grav})^2 \, v \rangle \approx 4\pi R^2 \sigma_{\rm B} (2000 \,{\rm K})^4. \tag{5}$$

Therefore measured (unredshifted) surface temperatures of nearby NSs below about 2000K can start to constrain short-range interactions of DM with NS matter. Conversely, finding several old isolated neutron stars with temperatures of order 2000K and greater near our Galactic radius—with higher temperatures in DM-rich regions—could be a sign of DM kinetic heating.

We now consider a long-range (> 20 km) fifth force, which changes the heating rate calculation, Eq. (4), in three ways. First, more DM is focussed and potentially captured by the NS (larger b_{max}).⁴ Second, the DM's kinetic energy near the NS surface—roughly equivalent to the DM-NS binding energy—is larger, meaning more energy is dissipated in a DM capture process (larger ΔE).⁵ Third, the energy deposition mechanism is qualitatively different due both to the long-range force and ultrarelativistic DM speeds at the NS surface; collective excitations of NS matter are particularly important.

We divide DM contributing to heating into two groups:

A. *Grazing* DM, including NS-transiting DM that is not gravitationally captured, as well as gravitationally bound DM whose first orbital period after capture is greater than the NS lifetime, implying no subsequent energy deposits within the NS's lifetime.

⁴ A repulsive interaction would defocus DM and reduce the maximum possible kinetic heating rate. Here we focus on the attractive case.

⁵ Similar effects on Earth could be relevant for direct detection, and were discussed in [52, 53].

B. Captured DM, which deposits sufficient energy to become gravitationally bound on its first transit and deposits further energy on subsequent transits within the NS lifespan.

The total heating rate for a long-range interaction is thus

$$\dot{E}_{\rm kin} \approx \dot{E}_{\rm graze} + \dot{E}_{\rm cap}$$
 (6)

with $\dot{E}_{\rm graze} \approx \dot{N}_{\rm graze} \Delta E_{\rm graze}$ and $\dot{E}_{\rm cap} \approx \dot{N}_{\rm cap} \Delta E_{\rm cap}$. Below in Secs. II A-II B, we derive explicit estimates of $\Delta E_{\rm graze}$, $\dot{N}_{\rm graze}$, $\Delta E_{\rm cap}$, and $\dot{N}_{\rm cap}$ in Eqs. 7, 12, 16, and 19, respectively. Then in Sec. II C we discuss the maximal heating rate, analogous to Eq. 5, requiring assistance by additional short-range forces. In Sec. II D we estimate when heating is effectively continuous and possibly destructive to the NS, which is relevant at the higher mass scales we consider. Finally, in Sec. II E, we present limits based on our estimates and Eq. 3.

A. Grazing heating rate

1. $\Delta E_{\rm graze}$

Two stars in a close encounter can become bound by sinking energy and angular momentum into seismic oscillations of the stars through gravitational tidal forces [54, 55]. Pani and Loeb [56] considered a similar capture mechanism for primordial black holes (PBHs) by NSs. They modeled PBHs as point-like objects that remain intact as they transit the NS, and found that tidally deposited energy exceeds energy deposit through dynamical friction by several orders of magnitude. A small, compact DM object should behave similarly, and an additional Yukawa force with range much larger than the NS radius will simply effectively increase the strength of the gravitational tidal forces by a factor $1 + \tilde{\alpha}$.

Based on [56], we estimate the energy deposited through tidal excitation of NS seismic oscillations by DM that transits an NS as

$$\Delta E_{\text{graze}} \approx \frac{Gm_X^2 (1+\tilde{\alpha})^2}{R} 4\sqrt{l_{\text{max}}}$$
(7)

where l_{max} corresponds to the largest spherical seismic mode excited in the NS. Qualitatively, thinking of the NS like a spring, the energy goes as the square of the amplitude of the oscillation, which is set by the maximum tidal force at close approach—proportional to $(1 + \tilde{\alpha})m_X$. The stiffness of the NS equation of state determines the nontrivial dependence on mode number. We refer the reader to [56] for details.

Ref. [56] considers many possible cutoffs for l_{max} . The limiting cutoffs come from demanding the particle size, R_X , is smaller than the mode's wavelength, leading to $l_{\text{max}} < R/R_X$, and that the DM crossing time, $\tau_{\text{cross}} \sim R/\beta_R \sim R$, is short compared to the shear viscosity oscillation damping timescale [57],

$$\tau_{\eta} \approx \frac{\rho R^2 / \eta}{(l-1)(2l+1)},\tag{8}$$

where η is the shear viscosity, and ρ is the mass density of the NS. For cold NSs with $T < 10^8 \text{K}$, in which neutrons and protons are expected to be superfluid (at least outside the inner core of the NS, where the tidally-induced oscillations are supported) the dominant source of viscosity is from electron scattering, η_e [58]. To within an order of magnitude, for a given temperature, the maximal value of η_e/ρ occurs around $\rho \sim 10^{10}$ –4 × $10^{14} \frac{\text{g}}{\text{cm}^3}$, and is [59, 60]

$$\left(\frac{\eta_e}{\rho}\right)_{\text{max}} \approx \left(\frac{T}{10^8 \text{K}}\right)^{-2} 10^4 \text{cm}^2/\text{sec},$$
 (9)

leading to an estimate

$$l_{\text{max}} \sim \min\left(10^2 \left(\frac{T}{10^4 \text{K}}\right), \frac{R}{R_X}\right)$$
 (10)

for DM that is relativistic (and ultrarelativistic) at the NS surface, with the consistency requirement, $l_{\text{max}} > 1$. For simplicity and consistency, we consider only DM and NSs with

$$\frac{R_X}{R} < 10^{-2} \frac{10^4 \text{K}}{T} < 1$$
 and $T < 10^8 \text{K}$ (11)

such that the shear viscosity timescale determines the highest excited mode number. For maximally compact DM objects, this requires $m_X \lesssim 10^{-2} \frac{10^4 \text{K}}{T} M_{\odot} < M_{\odot}$. The cutoff occurs at lower mass for less compact DM.

A few other factors deserve mention. First, our estimate based on [56] is consistent only if both the DM and NS survive the DM's transit. For DM to survive, the Roche distance—where the tidal forces on the DM from the NS start to exceed the binding forces—must be smaller than the NS radius. Depending on the forces binding the DM, the DM must be sufficiently compact.⁶ Energy deposits comparable to a few percent of the NS's gravitational binding energy could also destroy the NS. We discuss this case further in Secs. IIB1 and IID.

⁶ Modeling the DM binding force per mass as proportional to $\frac{(\tilde{\alpha}_{\chi,\text{eff}}+1)Gm_X}{R_X^2}$ on the DM surface, given $R_X \ll R$, the Roche distance is approximately $r_{\text{Roche}} \sim \left(4\frac{(1+\tilde{\alpha})M}{(1+\tilde{\alpha}_{\chi,\text{eff}})m_X}\right)^{1/3}R_X$, and in terms of the DM and NS compactnesses, the DM can survive only if $\frac{Gm_X}{R_X} > 4\frac{(1+\tilde{\alpha})M}{(1+\tilde{\alpha}_{\chi,\text{eff}})}\frac{GM}{R}\left(\frac{R_X}{R}\right)^2$.

Second, the estimate Eq. 7 is based on analyzing a particle's infall from rest. But as discussed in [56], it should be a decent estimate for particles with other trajectories as long as they breach or come close to breaching the NS surface. On the other hand, at distances, r, large compared to R, the tidal force falls off as r^{-3} and effective crossing times lengthen when $r_{\min} \gg R$. Indeed estimates of gravitational tidal capture for close star encounters as in [54] apply in this case, and the moral is that a good estimate of heating and capture comes from counting only DM that intersects the NS, with ΔE_{graze} as in Eqs. 7 and 10 for all such DM.

2. $\dot{N}_{\rm graze}$

The number of DM particles of mass m_X and asymptotic mass density ρ_X passing through a given NS per time—the flux—is

$$\dot{N}_{\text{graze}} = \frac{\rho_X}{m_X} \pi \langle b_{\text{max}}^2 v \rangle. \tag{12}$$

Given focusing through gravity alone, $\dot{N}_{\rm graze} \sim \frac{10^{-24}}{\rm yr} \frac{\rho_X}{0.4\,{\rm GeV/cm^3}} \left\langle \frac{10^{-3}}{v} \right\rangle \frac{M_\odot}{m_X} \frac{R}{10\,{\rm km}} \frac{GM}{2\,{\rm km}}$. An attractive DM-NS fifth force focuses more DM onto a NS, leading to a significantly larger flux via larger $b_{\rm max}$. For moderate $\tilde{\alpha}$ and $\lambda \gg R$, compared to focusing through gravity alone, $b_{\rm max}$ is larger by a factor $\sqrt{1+\tilde{\alpha}}$. When $\tilde{\alpha}\gg 1$, $b_{\rm max}$ grows linearly with $\tilde{\alpha}$ until a cutoff where an *outer* centrifugal barrier at $r>\lambda$ from the exponential turn-on of the fifth force becomes stronger than the always-present *inner* centrifugal barrier. More specifically, when $\tilde{\alpha}\gg 1$,

$$b_{\text{max}}v \sim \begin{cases} GM\tilde{\alpha} & \text{inner barrier} \\ \sqrt{2GM\lambda\log\left(\tilde{\alpha}\log\tilde{\alpha}\right)} & \text{outer barrier when } \tilde{\alpha}e^{-GM/\lambda v^2} < 1 \\ \lambda v\log\left(\frac{\tilde{\alpha}GM}{\lambda v^2}\right) & \text{outer barrier otherwise,} \end{cases}$$
(13)

with $b_{\text{max}} = \min(b_{\text{max,inner}}, b_{\text{max,outer}})$ if $\tilde{\alpha}GM/\lambda v^2 \gtrsim e$ and $b_{\text{max}} = b_{\text{max,inner}}$ otherwise. In Appendix A, we derive the general relativistic equation of motion that determines b_{max} in Eqs. A2-A5 along with analytic approximations in Eqs. A6-A8; Fig. 6 shows our analytic approximations alongside numerical solutions to the exact barrier-determining expressions.

B. Captured heating rate

1. $\Delta E_{\rm cap}$

The energy deposited per DM particle captured is approximately the DM kinetic energy at the NS surface,

$$E_{\rm DM, \, kin}(R) \approx m_X(\gamma_R - 1).$$
 (14)

with

$$\gamma_R = \frac{\frac{1}{\sqrt{1 - v^2}} + \tilde{\alpha} \frac{GM}{R} e^{-R/\lambda}}{\sqrt{1 - \frac{2GM}{R}}} \approx \frac{1 + \frac{GM}{R} \tilde{\alpha} e^{-R/\lambda}}{\sqrt{1 - \frac{2GM}{R}}} \approx 1 + \frac{GM}{R} \left(1 + \tilde{\alpha} e^{-R/\lambda} \right) \tag{15}$$

as measured in a locally flat frame at the NS surface. Since DM asymptotic speeds, v, are generally much less than the escape speed at the NS surface, the energy deposit is essentially independent of v. Without a fifth force, for typical neutron stars, $\gamma_R \sim \sqrt{5/3}$. With a fifth force, $\gamma_R - 1$ is larger by about a factor of $1 + \tilde{\alpha}e^{-R/\lambda}$.

If the period of the first orbit after capture, Δt_1 , is greater than NS lifetime, then the DM deposits only energy ΔE_{graze} within the NS lifetime. Hence we estimate

$$\Delta E_{\rm cap} \approx \left(\frac{\Delta E_{\rm graze}}{E_{\rm DM, \, kin}(R)}\right)^{\Delta t_1/t_{\rm NS}} E_{\rm DM, \, kin}(R) \qquad (\text{when } \Delta E_{\rm graze} \ll E_{\rm DM, \, kin}(R))$$
 (16)

to account for the timescale for captured DM to deposit further energy; specifically, Eq. 16 counts the entire available energy of captured DM in the heating rate only when $\Delta t_1 \ll t_{\rm NS}$, and the heating rate cuts off when $\Delta t_1 > t_{\rm NS}$. In this latter case, the DM is counted as "grazing" DM.⁷ We estimate the orbital period in Appendix B; see Δt_1 in Eqs. (B4)-(B5).

Using Eqs. 7, 10, 14, and 15, we see $\Delta E_{\rm graze} < E_{\rm DM, \, kin}(R)$ as long as $\frac{m_X}{M}(1+\tilde{\alpha})40\sqrt{\frac{T}{10^4{\rm K}}} < 1$. The condition saturates when $\Delta E_{\rm graze} \approx E_{\rm DM, \, kin}(R) \approx \sqrt{\frac{10^4{\rm K}}{T}} \frac{1}{40} \frac{GM^2}{R}$, or when the energy deposit is about 10% of the NS binding energy ($\sim \frac{3}{5} \frac{GM^2}{R}$) given $T \sim 42,000{\rm K}$. We expect such an energy deposit to destroy the NS rather than "heat" it, as we will discuss further in Sec. II D. Therefore $\Delta E_{\rm graze} < E_{\rm DM, \, kin}(R)$ holds as long as the kinetic heating limit is relevant.

⁷ Note the first energy deposit of captured DM is double counted in $\dot{E}_{\rm graze}$ and $\dot{E}_{\rm cap}$, which is acceptable for an order-of-magnitude estimate since it will at most overestimate the heating effect by a factor of two, and in most cases by a only a tiny fraction over one.

2. $\dot{N}_{\rm cap}$

To become gravitationally bound to the NS, DM must lose sufficient energy when it first grazes the NS surface. Thus the capture rate is approximately

$$\dot{N}_{\rm cap} \approx \frac{\rho_X}{m_X} \pi \langle b_{\rm max}^2 v \rangle_{v < v_{\rm cap}},$$
 (17)

where the average is over asymptotic DM speeds up to a the maximum speed of DM that is captured:

$$v_{\rm cap} = \sqrt{2\Delta E_{\rm graze}/m_X}.$$
 (18)

Given a Maxwellian velocity distribution with peak speed v_p , since $(b_{\text{max}}v)$ is nearly constant as function of v—increasing negligibly for most or our parameter range of interest and less than linearly in the entire range—to reasonable approximation,

$$\dot{N}_{\rm cap} \approx \frac{\rho_X}{m_X} \pi (b_{\rm max} v)^2 |_{v \to \min(v_p, v_{\rm cap})} \frac{2}{\sqrt{\pi} v_p} f \tag{19}$$

where

$$f \approx \left(1 - e^{-v_{\text{cap}}^2/v_p^2}\right) \tag{20}$$

roughly represents the fraction of surface-breaching DM that is captured. We can also use Eq. (19) to estimate $\dot{N}_{\rm graze}$ by taking $v_{\rm cap} \to 1$.

C. Capture assisted by short-range interactions

We have just described a capture mechanism through DM's tidal force excitation of seismic oscillations in an NS—classical collective modes stretching over the entire NS. In contrast, most previous treatments of kinetic heating have focussed on effectively local interactions of DM with one or more individual nucleons or leptons within the NS during a transit [28–47]. A notable exception is [61], which focuses specifically on collective effects within dense stellar media in DM scattering.

Relative to the case without a fifth force, when the fifth force increases DM's speeds in the NS rest frame (c.f. Eq. 15), the kinematic upper limit on energy transfer to nucleons in elastic DM-nucleon interactions also increases. At the same time, length contraction of the NS in the DM-nucleon CM frame can be significant, so it is easier for the de Broglie wavelength of the CM motion $(q^{-1} \sim 1/\sqrt{2m_n\Delta E_{\text{graze}}})$ to be larger than the inter-nucleon distance along

the direction of motion in the CM frame. Thus while the increased CM energy might naively increase nucleon-DM elastic cross sections, the range of kinematically allowed energies where nucleons are effectively free is also narrower. When the DM is ultrarelativistic at the NS surface, we expect proper treatment of collective effects in NS matter to be particularly important in a treatment of DM scattering via short-range forces.

Rather than trying to model specific short-range interactions and account for the relevant microscopic NS physics that determines the probability of capture, we consider maximal heating, where an order one fraction of transiting DM is captured. In this case,

$$\dot{E}_{\rm kin, \ max} \approx E_{\rm DM, \ kin}(R) \dot{N}_{\rm graze}$$
 (21)

with $E_{\rm DM,\;kin}(R)$ given by Eq. 14 and $\dot{N}_{\rm graze}$ by Eq. 12.

D. Cooling timescale and continuous heating approximation

NSs are born with internal temperatures of order 10¹¹ K and rapidly cool through neutrino and photon emission to under 10⁷ K within about 1000 years. Without additional sources of heating, NSs are expected to cool to under 1000 K within about 20 Myr (see *e.g.* [62, 63]). Under temperatures of order 10⁶ K, photon emission dominates, and nucleons in at least the inner crust and outer core of such cold stars are thought to be superfluid. The heat capacity (per unit volume) of such very cold NS's is dominated by ultrarelativistic, degenerate electrons, and is given by [64]

$$c_{V,e} \approx \frac{p_{\rm Fe}^2 k_{\rm B}^2 T}{3} = \frac{(3\pi^2 n_e)^{2/3} k_{\rm B}^2 T}{3}.$$
 (22)

Given heating only through DM kinetic heating, and black-body-radiation-dominated cooling, the NS temperature evolves in time according to

$$C_V \frac{dT}{dt} = \dot{E}_{\rm kin} - 4\pi R^2 \sigma_B T^4. \tag{23}$$

Without a heat source, using the relations above and approximating the NS as roughly uniform temperature throughout, we approximate the timescale to cool from a higher temperature T_h to a lower temperature of order T_l below 10⁶K as

$$t_{\rm c}(T_l) \sim \frac{R(3\pi^2 n_e)^{2/3} k_{\rm B}^2}{18\sigma_B T_l^2} \left(1 - \left(\frac{T_l}{T_h}\right)^2\right) \sim 10^4 \,\mathrm{yr} \left(\frac{10^4 \mathrm{K}}{T_l}\right)^2 \left(1 - \left(\frac{T_l}{T_h}\right)^2\right)$$
 (24)

where we set the electron density to a typical value in the NS outer core, $n_e \sim 0.01 \text{fm}^{-3}$. To set a kinetic heating limit based on a maximum temperature, T, we require a deposit rate (flux) comparable to or greater than one per cooling time, $\dot{N} \gtrsim 1/t_c(T)$.

Going the other way, the temperature, T_h , to which a NS is heated from temperature T_l through an energy deposit ΔE is given by

$$\Delta E = \int C_V dT \sim \frac{4\pi R^3}{3} \frac{(3\pi^2 n_e)^{2/3} k_{\rm B}^2}{6} (T_h^2 - T_l^2) \sim 5 \times 10^{-14} \frac{GM^2}{R} \frac{T_h^2 - T_l^2}{(10^6 \text{K})^2}$$
(25)

where the last expressions apply when both temperatures are below 10^6 K. The heat capacity rises by a factor of 20 or so at higher temperatures, and we can see that $\Delta E \gtrsim 10^{-2} \frac{GM^2}{R}$, approaching the gravitational binding energy of a NS, roughly heats a NS back above its temperature at birth ($\sim 10^{11}$ K). We expect a single energy deposit of order $10^{-2} \frac{GM^2}{R}$ or greater to destroy a NS. So the mere existence of a cold NS of age $t_{\rm NS} > \dot{N}_{\rm cap}^{-1}$ limits

$$\frac{\Delta E_{\text{graze}}}{10^{-2}GM^2/R} \sim 10^4 \left(\frac{m_X}{M}\right)^2 (1+\tilde{\alpha})^2 \sqrt{\frac{T}{4.2\text{kK}}} < \frac{E_{\text{DM, kin}}(R)}{10^{-2}GM^2/R} \sim 10^2 \frac{m_X}{M} (1+\tilde{\alpha}) < 1. \quad (26)$$

E. Limits

Here we present limits based on Eq. 3 for the coldest presently known NS [48], a slow, isolated pulsar located about 170 pc from Earth, with temperature $T_{\rm s,i_{max}}^{\rm meas} = 42,000\,\rm K$ and age $t_{\rm NS} = 0.3\,\rm Gyr$. Without additional sources of heating, this NS should have cooled to temperatures below 1000 K within the first 10% of its life. The four panels in Fig. 2 show limits for four different force ranges, λ , spanning our range of interest. The thick black tidal heating limit lines result from our estimate of $\dot{E}_{\rm kin}$ in Eq. 6, as described in Secs. II A-II B. The thick red maximal kinetic heating line results when an order one fraction of NS-transiting DM deposit their entire available energy over a NS lifetime, with a heating rate as in Eq. 21, requiring assistance from short-range forces as described in Sec. II C. We employed our analytic estimate of the impact parameter in Eqs. A6-A8 to calculate the relevant fluxes (Eqs. 12 and 19), and the limits assume asymptotic DM density $\rho_X = 0.4\,\rm GeV/\,cm^3$, a Maxwellian speed distribution peaked at $v_p \sim 10^{-3}$, and typical NS parameters $\frac{GM}{R} \approx 0.2$, $R \approx 10\,\rm km$. Below we explain the scaling of the limits, starting with the high-mass behavior and working to lower masses.

To set a limit based on Eq. 3 for a given maximum NS temperature T, we require the frequency of energy deposit events, \dot{N} , to be comparable to or greater than the inverse

cooling timescale, $1/t_c(T)$, in Eq. 24. This requirement determines the high-mass cut-off for the limit, shown by the thin purple "flux <1/(cooling time)" lines in Fig. 2. Using Eq. 12, and assuming a Maxwellian speed distribution with peak speed v_p , the high-mass limit reads,

$$\dot{N}_{\text{graze}} t_{\text{c}} \sim 6 \times 10^{-22} \left(\frac{t_c}{500 \,\text{yr}}\right) \left(\frac{R}{10 \,\text{km}}\right)^2 \left(\frac{10^{-3}}{v_p}\right) \left(\frac{M_{\odot}}{m_X}\right) \left(\frac{(b_{\text{max}} v)|_{v_p}}{R}\right)^2 < 1.$$
 (27)

where fiducial quantities in the parentheses are used to obtain our Fig. 2 and we have taken here (and throughout) $\rho_X = 0.4 \text{ GeV/cm}^3$. Note that $t_c(T_l = 42 \text{ kK}) \sim 500 \text{ years according}$ to Eq. 24. Here, b_{max} is given in Eqs. A6-A8 and Fig. 6, and its scaling with $\tilde{\alpha}$ depends on whether it is determined by the inner or outer barrier, as indicated by the brown horizontal dashed lines in the figure.⁸ Eq. 13 gives the scaling of b_{max} in various regimes.

The grazing and capture fluxes are approximately equal at the highest constrained masses, where $v_{\rm cap} \sim 5(1+\tilde{\alpha}) \left(\frac{m_X}{M_\odot}\right)^{1/2} \left(\frac{T}{42\,{\rm kK}}\right)^{1/4} \left(\frac{10\,{\rm km}}{R}\right)^{1/2} \gtrsim v_p$ (see Eqs. 7, 10, and 18). The tidal heating limit curves break away from the $\dot{N}_{\rm graze} = 1/t_{\rm c}$ curves where $v_{\rm cap} < v_p$, below the dashed blue lines in Fig. 2. When $v_{\rm cap} < v_p$, the flux-limited limit follows

$$\dot{N}_{\rm cap} t_{\rm c} \sim 10^{-14} (1 + \tilde{\alpha})^2 \left(\frac{t_c}{500 \,\text{yr}}\right) \left(\frac{R}{10 \,\text{km}}\right) \left(\frac{T}{42 \,\text{kK}}\right)^{1/2} \left(\frac{10^{-3}}{v_p}\right)^3 \left(\frac{(b_{\rm max} v)|_{v_{\rm cap}}}{R}\right)^2 < 1.$$
(28)

For lower masses, the limit applies in parameter regions with continuous heating, and when $\dot{E}_{\rm cap} \gg \dot{E}_{\rm graze}$ (see Eqs. 6, 7, 12, 16, and 19), the limit reads

$$\frac{\dot{E}_{\text{cap}}}{L_{\circ}} \sim 2 \times 10^{2} (1 + \tilde{\alpha})^{3} \left(\frac{M}{1.4 \, M_{\odot}}\right) \left(\frac{T}{42 \, \text{kK}}\right)^{1/2} \left(\frac{10 \, \text{km}}{R}\right)^{2} \left(\frac{10^{-3}}{v_{p}}\right)^{3} \left(\frac{m_{X}}{M_{\odot}}\right) \left(\frac{(b_{\text{max}} v)|_{v_{\text{cap}}}}{R}\right)^{2} < \left(\frac{T_{\text{s,}i_{\text{max}}}}{42 \, \text{kK}}\right)^{4},$$
(29)

where $L_{\circ} = 4\pi R^2 \sigma_B (42 \text{kK})^4$, and the scaling of $(b_{\text{max}} v)|_{v_{\text{cap}}}$ with $\tilde{\alpha}$ again depends on whether the outer or inner barrier determines b_{max} . For Fig. 2, the relevant relationships are $b_{\text{max}} v \sim GM\tilde{\alpha}$ for the inner barrier and $b_{\text{max}} v \sim \sqrt{2GM\lambda \log(\tilde{\alpha}\log\tilde{\alpha})}$ for the outer.

The thin green "period > NS age" lines in Fig. 2 are the contours $\Delta t_1 = t_{\rm NS}$ with Δt_1 as in Eq. B6. Heating from captured DM goes to zero when $\Delta t_1 > t_{\rm NS}$ (c.f. Eq. 16), explaining why the limit asymptotes to this contour in the first three panels of Fig. 2 at low DM masses.

⁸ In the first three panels, we show the transition for $b_{\text{max}}|_{v_{\text{cap}}}$ and in the last the dashed line corresponds to the transition for $b_{\text{max}}|_{v_p}$.

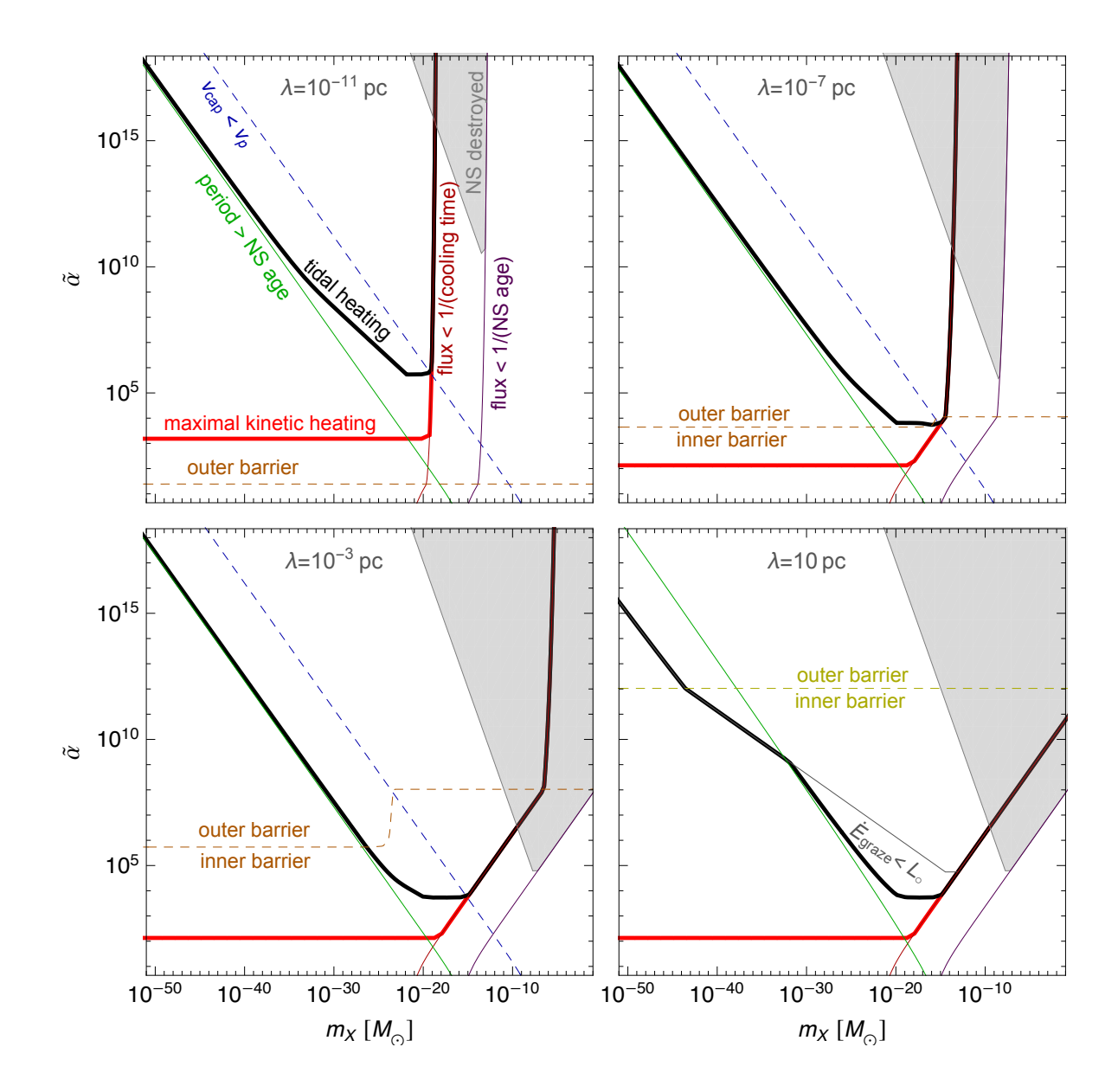


FIG. 2. Limit on an attractive NS-DM fifth force (Eq. 1) for four representative force ranges, λ , from *tidal* kinetic *heating* of the coldest known NS with temperature T < 4.2 kK and age 0.3 Gyr (black). In Sec. II E we explicitly explain how limits were derived in several regimes, beginning at high mass. Eqs. 27, 28, 29, and 30 determine the limits in the first three panels from high to low mass, respectively, and Eq. 31 applies at the lowest masses in the last panel. The thick red maximal kinetic heating curve assumes 100% of transiting DM is captured and deposits energy quickly through additional short-range forces, leading to Eq. 32 at low masses. In the gray regions, the old NS would have been destroyed by a single DM encounter (see Eq. 26).

Using the results in Appendix B, for $\lambda \ll (\sqrt{GM}t_{\rm NS})^{2/3} \sim 10\,{\rm pc}\left(\frac{t_{\rm NS}}{\rm Gyr}\right)^{2/3}$, the $\Delta t_1 > t_{\rm NS}$ asymptote corresponds to

$$\frac{t_{\rm NS}}{\Delta t_1} = \frac{t_{\rm NS}}{GM} \frac{\sqrt{2}}{\pi} \left(\frac{\Delta E_{\rm graze}}{m_X}\right)^{3/2}
\approx 3 \times 10^{22} (1 + \tilde{\alpha})^3 \left(\frac{T}{42 \,\text{kK}}\right)^{3/4} \left(\frac{1.4 \,M_{\odot}}{M}\right) \left(\frac{10 \,\text{km}}{R}\right)^{3/2} \left(\frac{t_{\rm NS}}{0.3 \,\text{Gyr}}\right) \left(\frac{m_X}{M_{\odot}}\right)^{3/2} < 1.$$
(30)

In the last panel, at low masses the contour is instead controlled by heating from grazing encounters. When $\dot{E}_{\rm graze} \gg \dot{E}_{\rm cap}$, the limit is,

$$\frac{\dot{E}_{\text{graze}}}{L_{\circ}} \sim 4 \times 10^{-4} (1 + \tilde{\alpha})^{2} \left(\frac{T}{42 \,\text{kK}}\right)^{1/2} \left(\frac{10 \,\text{km}}{R}\right) \left(\frac{10^{-3}}{v_{p}}\right) \left(\frac{m_{X}}{M_{\odot}}\right) \left(\frac{(b_{\text{max}} v)|_{v_{p}}}{R}\right)^{2} < \left(\frac{T_{\text{s,i}}_{\text{max}}^{\text{meas}}}{42 \,\text{kK}}\right)^{4} \tag{31}$$

with $(b_{\text{max}}v)|_{v_p}$ as in Eq. 13 for large $\tilde{\alpha}$. The thin gray " $\dot{E}_{\text{graze}} < L_{\circ}$ " contour in the last panel corresponds to saturation of Eq. 31 evaluated at the fiducial parameters.

When an order one fraction of transiting DM is captured and deposits its available energy quickly, kinetic heating is "maximal." When $\lambda \gg R$ and $\dot{N}_{\rm graze}t_{\rm c} > 1$, the limit reads

$$\frac{\dot{E}_{\text{kin, max}}}{L_{\circ}} \sim 6 \times 10^{-6} (1 + \tilde{\alpha}) \left(\frac{M}{1.4 \, M_{\odot}}\right) \left(\frac{10 \, \text{km}}{R}\right) \left(\frac{10^{-3}}{v_p}\right) \left(\frac{(b_{\text{max}} v)|_{v_p}}{R}\right)^2 < \left(\frac{T_{\text{s,i}}_{\text{max}}^{\text{meas}}}{42 \text{kK}}\right)^4.$$
(32)

To one significant figure the maximal kinetic heating limit shown in red in Fig. 2 corresponds to

$$\tilde{\alpha} < 150$$
 when $\lambda \gtrsim 10^{-10} \text{pc}$, (33)

$$\frac{\lambda}{R}\tilde{\alpha}\log\left(\tilde{\alpha}\log(\tilde{\alpha})\right) < 4 \times 10^5$$
 when $R < \lambda \lesssim 10^{-10} \mathrm{pc}$. (34)

In Appendix C, we show that the kinetic heating limit above also rules out the possibility of observable pulsar glitches caused by angular momentum deposits of transiting DM.

Near-future measurements with infrared telescopes such as JWST should be able to improve NS surface temperature measurements by a factor of ten or better (see [28]). For smaller force ranges, tidal heating limits will not change much because they are bounded by the flux and energy deposit timescales (see Eqs. 27, 28 and 30) except in a narrow mass range, where Eq. 29 applies. The bound for larger λ will tighten at lower masses, according

to Eq. 31. If the temperature of a cold NS were an order of magnitude lower, so $T_s \sim 4,200$ K, the maximal kinetic heating limit (Eq. 32) becomes $\tilde{\alpha} \lesssim 2$ for all $\lambda \gtrsim R$. Recalling that the maximum heating rate of a typical local NS by DM focussed through gravity alone corresponds to $T_s \sim 2,000$ K (see Eq. 5), we expected maximal kinetic heating to constrain a fifth force to gravitational strength or weaker for temperatures approaching this infrared range.

We now highlight some important caveats. First, DM-DM interactions become important to NS capture and heating at time t_{eq} when the effective charge of captured DM is comparable to the effective charge of baryons in the NS:⁹ $\dot{N}_{cap}t_{eq}g_X = \frac{M}{m_n}g_n$. Accelerated (decelerated) capture and heating start just before t_{eq} given scalar (vector) mediation. Therefore scalar-mediated constraints should tighten and vector mediated constraints should loosen when

$$\frac{t_{\rm NS}}{t_{\rm eq}} = \frac{m_X}{M} \frac{\tilde{\alpha}}{\tilde{\alpha}_n} \dot{N}_{\rm cap} t_{\rm NS} > 1. \tag{35}$$

When this inequality is satisfied, time dependence of capture and heating rates should be taken into account. More specifically, the capture luminosity constraint, $E_{\rm DM, \, kin}(R) \dot{N}_{\rm cap} \approx m_X \frac{GM}{R} (1 + \tilde{\alpha}) \dot{N}_{\rm cap} < L_{\circ} \left(\frac{T_{\rm max}}{42 {\rm kK}}\right)^4$, is saturated in a region of parameter space with $t_{\rm eq} < t_{\rm NS}$ when

$$\frac{1+\tilde{\alpha}}{\tilde{\alpha}}\tilde{\alpha}_n < \frac{L_{\circ}t_{\rm NS}}{GM^2/R} \left(\frac{T_{\rm max}}{42{\rm kK}}\right)^4 \approx 4 \times 10^{-11} \left(\frac{t_{\rm NS}}{0.3\,{\rm Gyr}}\right) \left(\frac{T_{\rm max}}{42{\rm kK}}\right)^4. \tag{36}$$

Since WEP tests suggest $\tilde{\alpha}_n \lesssim 10^{-11}$ when $\lambda \gtrsim 2R_{\rm Earth}$ [11, 12, 65], DM-DM interactions may thus be relevant when $\tilde{\alpha}_n$ is significantly below this bound. Our kinetic heating limits which neglect DM-DM interactions are thus conservative in the scalar-mediated case since captured DM could further accelerate capturing more DM. On the other hand our bounds could lift in the vector-mediated case if the DM-DM repulsive interaction was sufficiently strong compared to the attractive DM-baryon interaction. Furthermore, heating that appears to accelerate (decelerate) at a characteristic timescale depending on local DM density and NS age could be a smoking gun signal of a scalar (vector) mediated long-range force.

We also remind the reader of restrictions necessary for consistency of our tidal heating estimate discussed in Secs. II A-II B. First, the DM must be sufficiently compact to survive an NS transit and to tidally excite modes up to the cutoff determined by shear viscous damping

⁹ This expression assumes the charge-to-mass ratio of captured DM is similar to that of halo DM. If this were untrue, additional heat would be released (absorbed) in the capture process, leading to larger (smaller) DM charge-to-mass ratios.

(see Sec. II A 1). Second, tidal energy deposits approach the expected maximum $E_{\rm DM, \, kin}(R)$ at approximately the same $\tilde{\alpha}, m_X$ parameter range as they approach a few percent of the NS gravitational binding energy, where we expect transiting DM to destroy rather than heat the NS (see Eq. 26). Fig. 2 shows this region in gray.

III. LIMITS FROM PULSAR TIMING ARRAYS

The use of PTAs to probe DM substructure has been extensively studied [18, 23–25, 66–70]. To set upper limits on the fifth force strength, we analyse the data collected by NANOGrav [51] in their 11-year dataset [49, 50]. This analysis utilizes the software enterprise [71] developed by NANOGrav and closely follows the Bayesian inference framework developed in our previous work [27].

We commence with deriving the phase shift signals measured by an observer on Earth due to a transiting DM. The intrinsic pulsar phase, $\phi(t)$, is often modelled as a truncated power series in t

$$\phi(t) = \phi_0 + \nu t + \frac{1}{2}\dot{\nu}t^2, \qquad (37)$$

where ϕ_0 is the phase offset, ν is the pulsar frequency and $\dot{\nu}$ is its first derivative. Astrophysical signals such as Doppler shifts due to transiting DM manifest as deviations from the above timing model.

The phase shift $\delta\phi(t)$ is related to the frequency shift $\delta\nu(t)$ by $\delta\phi(t) = \int_0^t \delta\nu(t')dt'$. In the presence of an external potential Φ , the acceleration of the pulsar induces an observed frequency shift due to the Doppler effect, which is given by [24]

$$\frac{\delta\nu}{\nu} = \hat{d} \cdot \int \nabla\Phi dt \,, \tag{38}$$

where \hat{d} is the unit vector pointing from Earth to the pulsar. The fifth force potential is given by Eq. (1) and $\Phi(r) = V_{\text{Yuk}}(r)/M$, and its gradient is

$$\nabla \Phi(r) = \frac{Gm_X}{r^2} \left[1 + \tilde{\alpha} (1 + r/\lambda) e^{-r/\lambda} \right] \hat{r} . \tag{39}$$

To simplify these expressions, we perform the analysis in the pulsar rest frame and place the pulsar at the origin. We then write the DM position as $\vec{r}(t) = \vec{r}_0 + \vec{v}t$ with \vec{v} being the DM velocity. The two important timescales in this system are the time of closest approach, $t_0 = -\vec{r}_0 \cdot \vec{v}/v^2$, and the signal width, $\tau = |\vec{r}_0 \times \vec{v}|/v^2$. The impact parameter is given

by $\vec{b} = \vec{r_0} + \vec{v}t_0 = v\tau$. Defining the dimensionless time variable, $x \equiv (t - t_0)/\tau$, we write $\vec{r} = b(\hat{b} + x\hat{v})$ and $r = b\sqrt{1 + x^2}$. Using these variables, the frequency shift due to the fifth force can be written as

$$\left(\frac{\delta\nu}{\nu}\right)_{\text{fifth}} = \tilde{\alpha}Gm_X \frac{1}{v^2\tau} \hat{d} \cdot \int \frac{1}{(1+x^2)^{3/2}} \left(1 + \frac{b}{\lambda}\sqrt{1+x^2}\right) e^{-(b/\lambda)\sqrt{1+x^2}} (\hat{b} + x\hat{v}) dx \,. \tag{40}$$

The equivalent expression for gravitation is given by Eq. 40 but with $\tilde{\alpha} = 1$ and $\lambda \to \infty$. In general the integral in Eq. 40 has to be computed numerically. An additional integration over time gives the phase shift $\delta \phi(t)$.

The above analysis assumes that the DM trajectory is approximately a straight line, which has been shown to hold for the DM mass range that we are interested in for gravity only [27]. In the presence of a fifth force, the deviation in DM paths is small if and only if $b \approx r_{\min}$ where r_{\min} is the distance of closest approach. Eq. A4 implies $b \approx r_{\min}$ iff $\frac{GM}{bv^2}(1 + \tilde{\alpha}e^{-b/\lambda}) \ll 1$. One can estimate the minimum impact parameter of all passing DMs to be

$$b_{\min} \sim \left(\frac{3}{4\pi} \frac{m_X}{\rho_X}\right)^{1/3} \sim 3 \,\mathrm{pc} \left(\frac{m_X}{M_\odot}\right)^{1/3} \,.$$
 (41)

If the aforementioned condition is not satisfied, then DMs will substantially converge to the pulsar, which will lead to a larger amplitude for the timing deviation. Hence our constraints based on the straight-trajectory approximation serve as a conservative estimate. We leave a detailed analysis of PTA constraints accounting for full DM orbit information as a potential direction for future work.

To search for the DM signal in experimental data, similar to the static analysis in Ref. [27], we parametrize the signal with the leading order perturbation of the timing model

$$\frac{\delta\phi(t)}{\nu} = \frac{A}{\mathrm{yr}^2}t^3\,,\tag{42}$$

where A characterizes the signal amplitude. Terms of order t^2 or less are degenerate with the timing model and have no observable consequences. We search for the signal in Eq. 42 using enterprise and compute the Bayesian posterior distribution of the DM amplitude, $P(A|\delta \vec{t})$, using the Markov Chain Monte Carlo sampling techniques with the PTMCMCSampler package [72]. The parameters and priors are listed in Table. I. In particular, we adopt a uniform (instead of log-uniform) prior on the DM amplitude A, which is a standard procedure for upper-limit setting [27, 73]. For the red noise amplitude, however, we use a uniform prior

| Parameter | Description | Prior | Comments | | | |
|--------------------|------------------------------------|------------------------------------|--------------------------|--|--|--|
| | Red noise | | | | | |
| A_{red} | Red noise power-law amplitude | Log-Uniform $[-20, -11]$ | one parameter per pulsar | | | |
| $\gamma_{ m red}$ | Red noise power-law spectral index | Uniform $[0, 7]$ | one parameter per pulsar | | | |
| Dark Matter | | | | | | |
| A | Dark matter amplitude | Uniform $\pm [10^{-20}, 10^{-11}]$ | one parameter per pulsar | | | |

TABLE I. Parameters and priors used in the PTA analysis with the 11-yr dataset from NANOGrav. The notation Uniform $\pm[\ldots]$ stands for the union of Uniform $[+\ldots]$ and Uniform $[-\ldots]$. We account for the effects from white noise by marginalizing over a multiplicative pre-factor of the timing residual errors. Errors from Solar System ephemeris (SSE) modeling are corrected using BAYESEPHEM, as described in [50].

to avoid the transfer of signal power to the red noise process, which has been shown to lead to overstated Bayesian upper limits [74].

We now fix a choice of λ . To relate the posterior distribution $P(A|\delta \vec{t})$ to the fifth force parameters $\tilde{\alpha}$, we use a Monte Carlo simulation described in Ref. [27] to compute the conditional probability $P(A|\tilde{\alpha})$. In particular, we randomly distribute DMs in a sphere and compute the total $\delta \phi(t)$ using Eq. 40. We then numerically fit $\delta \phi(t)$ with a third order polynomial in t to extract the t^3 coefficient and hence A. This procedure is repeated for numerous realizations to obtain the required distribution $P(A|\tilde{\alpha})$. The final posterior distribution on $\tilde{\alpha}$ is then given by [27]

$$P(\tilde{\alpha}|\delta \vec{t}) \propto \prod_{i=1}^{N_P} \int_{-\infty}^{\infty} P(A_i|\tilde{\alpha}) P(A_i|\delta \vec{t}) dA_i$$
 (43)

where N_P is the number of pulsars.¹⁰ The posterior distribution satisfies the normalization condition $\int d\tilde{\alpha} P(\tilde{\alpha}|\delta \vec{t}) = 1$.

Finally, we compute the 90th percentile upper limit on $\tilde{\alpha}$ for each choice of λ , which is shown in Fig. 3. In the large mass limit, the constraints degrade since b_{\min} becomes $\frac{\text{larger than }\lambda}{\text{In Ref. [27]}}$ we also considered the possibility of deriving upper limits using the maximum amplitude among all pulsars (instead of using the amplitude in every single pulsar), but the limits turn out to be less stringent than the present results.

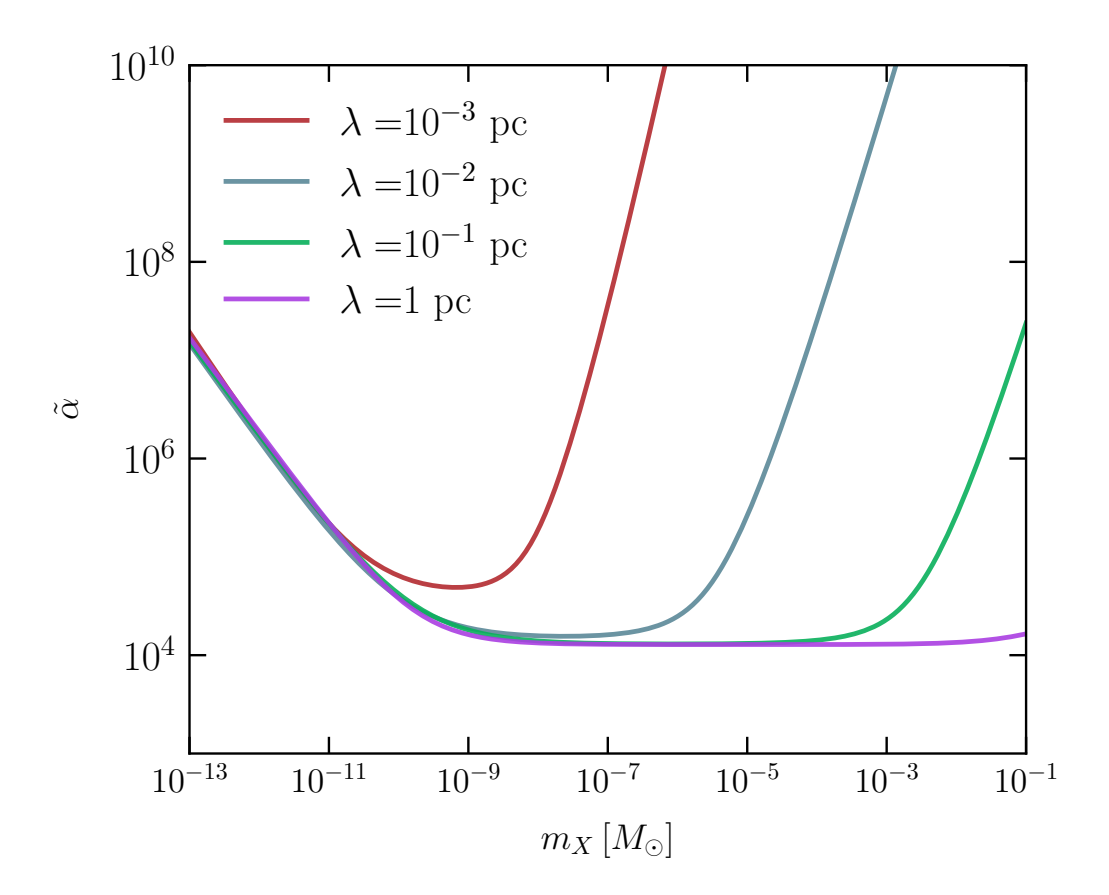


FIG. 3. The 90th percentile upper limits on the fifth force strength $\tilde{\alpha}$ derived from the NANOGrav 11-year dataset. The constraints are shown for different DM mass m_X and range λ .

sufficient to produce an observable signal. On the other hand, in the low mass limit, we have $b_{\min} \lesssim \lambda$, but the constraints also become less stringent, since the fifth force and gravitational strength weaken with the DM mass. For adequately large force ranges (i.e. $\lambda \gtrsim 10^{-2}$ pc), there is an intermediate mass regime where $b_{\min} \lesssim \lambda$ so the fifth force effectively modifies the gravitational constant by $G \to (1 + \tilde{\alpha})G$, but its strength is not enough to perturb the DM path, hence the constraints exhibit a plateau behavior similar to the gravity-only analyses in Ref. [27].

IV. INFERRED LIMITS FROM EQUIVALENCE PRINCIPLE TESTS AND THE BULLET CLUSTER

In this section we consider indirect constraints on a fifth force between NS matter and DM from a combination of weak equivalence principle (WEP) tests [1, 65], which can constrain

composition-dependent forces to be weaker than gravitational at macroscopic scales, and the bullet cluster bound on DM self-interactions [13, 14]. In Sec. IV A we translate a WEP bound on the differential acceleration of two baryonic bodies toward our Galaxy's center to a limit on $\tilde{\alpha}$ and λ when $\lambda \ll$ kpc. We then combine bullet cluster limits on $\tilde{\alpha}_X = g_X^2/4\pi G m_X^2$ with the very strong WEP constraints on $\tilde{\alpha}_n = g_n^2/4\pi G m_n^2$ at Earth and solar system scales $(\lambda \gtrsim 1000 \, \mathrm{km})$ to infer a limit on $\tilde{\alpha} = \sqrt{\tilde{\alpha}_X \tilde{\alpha}_n}$ in Sec. IV B. Our results are shown in Fig. 4.

A. Weak Equivalence Principle Tests

Most DM-baryonic matter WEP tests constrain the difference in acceleration between two baryonic test bodies (which we will label as A and B) toward the galactic center, divided by the total acceleration:¹¹ $\frac{\Delta a}{a_{\text{tot}}}$. When the total acceleration is dominated by gravity and the fifth force is Coulombic, assuming the DM charge-to-mass ratio is constant for DM throughout the halo, it is given by¹²

$$\frac{\Delta a_{\text{Coul}}}{a_{\text{tot}}} = \tilde{\alpha} \left[\left(\frac{Q}{M/m_n} \right)_A - \left(\frac{Q}{M/m_n} \right)_B \right], \tag{44}$$

where Q is the effective charge of the body in units of g_n . The difference in charge-to-mass ratio for the test bodies must be nonzero in order to obtain a non-trivial constraint. For normal matter, we consider couplings to baryon number or to B - L—i.e. Q = B or B - L, but other combinations lead to similar constraints.

To include range dependence in the differential acceleration calculation, we integrate over the force times DM distribution and correct Eq. 44 with the ratio $\frac{|\Delta \vec{a}_{\text{Yuk}}(\vec{r})|}{|\Delta \vec{a}_{\text{Coul}}(\vec{r})|}$. Given a spherically symmetric DM halo mass distribution, $\rho_{\text{halo}}(r')$, and a uniform DM charge-to-mass ratio, the net acceleration due to a Coulombic force from halo DM on object i at position \vec{r} relative to the halo's center is $\vec{a}_{\text{Coul}}(\vec{r}) = \tilde{\alpha} G \frac{Q_i}{M_i/m_n} \frac{\hat{r}}{r^2} \int_0^r \rho_{\text{halo}}(r') d^3 \vec{r}'$. For a Yukawa force, when $\lambda \ll r$, we find $\frac{13}{r}$

$$\vec{a}_{\text{Yuk}}(\vec{r}) = -\tilde{\alpha}G \frac{Q_i}{M_i/m_n} \vec{\nabla} \int_{\text{DM halo}} \frac{\rho_{\text{halo}}(r')e^{-|\vec{r}-\vec{r}'|/\lambda}}{|\vec{r}-\vec{r}'|} d^3 \vec{r}' \approx -4\pi \tilde{\alpha}G \lambda^2 \frac{Q_i}{M_i/m_n} \rho'_{\text{halo}}(r)\hat{r} . \tag{45}$$

¹¹ See Ref. [65] for one of the most highly cited treatments/reviews from the last decade.

¹² We neglect the difference between the atomic mass unit, u, and the neutron mass, m_n , throughout.

¹³ We dropped terms suppressed by $e^{-r/\lambda}$ and higher powers of $\frac{\lambda}{r}$. More precisely, we assumed $\lambda \rho'_{\rm halo}(r) \gg e^{-r/\lambda} \rho_{\rm halo}(r)$, $\frac{e^{-r/\lambda}}{r\lambda} \int e^{-r'/\lambda} \rho_{\rm halo}(r') r' dr'$, $\frac{\lambda}{r} \lambda^2 \rho''_{\rm halo}(r)$, . . .

| limit | ref | test (test objects) | $\Delta((B-L)/(M/m_n))$ | $\Delta(B/(M/m_n))$ |
|--|----------|-------------------------------------|-------------------------|---------------------|
| $\left \frac{\Delta a}{a_{\rm tot}} \right \lesssim 3 \times 10^{-4}$ | [75] | perihelion precession (Sun-Mercury) | 0.37 | ~ 0 |
| $\left \left \frac{\Delta a}{a_{\mathrm{tot}}} \right \lesssim 0.004 \right $ | [76] | binary pulsar (NS-WD) | 0.69 | 0.19 |
| $\left \left \frac{\Delta a}{a_{\rm tot}} \right \lesssim 10^{-5}$ | see [65] | lunar laser ranging (Earth-Moon) | 0.012 | ~ 0 |
| $\left \left \frac{\Delta a}{a_{\rm tot}} \right \lesssim 10^{-4}$ | [65] | torsion pendula (Be-Ti, Be-Al) | 0.013, 0.036 | 0.0024, 0.0020 |

TABLE II. Collection of limits on the differential acceleration of two baryonic test objects toward the galactic center. The B and B-L number to mass ratios are based on Table II in [75] and Table 1 in [65]. The magnitude of the gravitational acceleration field due to galactic dark matter at Earth was taken as 5×10^{-11} m/s² in [65], following [77]; this is the value assumed in calculating $\left|\frac{\Delta a}{a_{\rm tot}}\right|$ for the last two entries.

Therefore when $\lambda \ll r$ the ratio of Yukawa to Coulomb differential accelerations for test objects near the same radial distance, r, from the halo center is given by

$$\frac{|\Delta \vec{a}_{\text{Yuk}}(\vec{r})|}{|\Delta \vec{a}_{\text{Coul}}(\vec{r})|} \approx \frac{-4\pi r^4 \rho'_{\text{halo}}(r)}{\int_0^r \rho_{\text{halo}}(r') d^3 \vec{r}'} \left(\frac{\lambda}{r}\right)^2. \tag{46}$$

Given an NFW DM halo profile [78],

$$\rho_{\text{halo}}(r) = \frac{\rho_{\text{halo},0}}{r/r_s(1 + r/r_s)^2},\tag{47}$$

with scale radius r_s , the expression in Eq. (46) becomes

$$\frac{|\Delta \vec{a}_{\text{Yuk}}(\vec{r})|}{|\Delta \vec{a}_{\text{Coul}}(\vec{r})|} = \frac{(r/r_s)^2 (1 + 3r/r_s)}{(1 + r/r_s)^2 \left[(1 + r/r_s) \log(1 + r/r_s) - r/r_s \right]} \left(\frac{\lambda}{r}\right)^2. \tag{48}$$

The coefficient in Eq. (48) lies between 2.4 and 2.6 when $0.23 < \frac{r}{r_s} < 2$, with the maximum of about 2.6 occurring near $\frac{r}{r_s} = 0.8$. For concreteness we take $r = 8 \,\mathrm{kpc}$ and set the coefficient to 2.5, which is within 4% of the exact value when $4 \,\mathrm{kpc} < r_s < 35 \,\mathrm{kpc}$, well within agreement with recent fits [79, 80]. The constraint on a Yukawa fifth-force then reads,

$$\left| \frac{\Delta a_{\text{Yuk}}}{a_{\text{tot}}} \right| \approx 2.5 \,\tilde{\alpha} \left(\frac{\lambda}{r} \right)^2 \left[\left(\frac{Q}{M/m_n} \right)_A - \left(\frac{Q}{M/m_n} \right)_B \right] < \left| \frac{\Delta a}{a_{\text{tot}}} \right|^{\text{max}}. \tag{49}$$

Table II shows a variety of recent limits on differential accelerations, along with the difference in B- and (B-L)-to-mass ratios for the test objects. The strongest limit given Q=B corresponds to $\left|\frac{\Delta a}{a_{\text{tot}}}\right|/\left|\Delta\left[Q/(M/m_n)\right]\right|\lesssim 0.02$. The best limit given Q=B-L is more than

an order of magnitude stronger. Therefore the limit on a Yukawa fifth force coupling to baryon number from equivalence principle tests is roughly,

$$2.5\,\tilde{\alpha}\left(\frac{\lambda}{8\,\mathrm{kpc}}\right)^2 \lesssim 0.02$$
 when $\left(\frac{m_X}{\rho_X}\right)^{1/3} \ll \lambda \ll 8\,\mathrm{kpc}$, (50)

where the conditions on λ are necessary for consistency of our spherically symmetric fluid approximation for the DM distribution near Earth, where the inter-DM spacing is estimated as $\left(\frac{m_X}{\rho_X}\right)^{1/3}$ and we set Earth's galactic radius to $r \approx 8\,\mathrm{kpc}$.

B. Bullet Cluster limit

Following Ref. [15], the momentum transfer cross section for a long-range DM-DM interaction can be approximated as $\sigma_T \approx 4\pi d_C^2$ where d_C is the distance of closest approach given a repulsive Yukawa interaction, $V_{\rm Yuk} = \frac{G m_X^2 \tilde{\alpha}_X}{r} e^{-r/\lambda}$. For simplicity we assume an order one fraction of the DM by mass takes the form of objects with roughly the same size. Assuming the Yukawa DM-DM interaction is much stronger than the gravitational DM-DM interaction at closest approach, $\frac{d_C}{\lambda} = W\left(\frac{4G\tilde{\alpha}_X m_X}{\lambda v^2}\right)$, where W is the Lambert W function satisfying $W(z)e^{W(z)}=z$ and v is the relative speed of the interacting DM pair. Observation of the bullet cluster sets the rough limit $\frac{\sigma_T}{m_X}=\frac{4\pi d_C^2}{m_X}<\frac{\mathrm{cm}^2}{\mathrm{g}}$, translating to a limit

$$\frac{4G\tilde{\alpha}_X m_X}{v^2} < \sqrt{\frac{1}{4\pi} \frac{m_X}{g}} e^{\sqrt{\frac{1}{4\pi} \frac{m_X}{g}} \frac{\text{cm}}{\lambda}} \text{ cm}$$
 (51)

or

$$\tilde{\alpha}_X \sqrt{\frac{m_X}{M_{\odot}}} < 2 \times 10^6 \left(\frac{v}{10^{-2}}\right)^2 e^{4 \times 10^{-3} \sqrt{\frac{m_X}{M_{\odot}}} \frac{\text{pc}}{\lambda}}.$$
(52)

The limit becomes very weak when the interaction range, λ , is comparable or small compared to the scattering length $\sqrt{\frac{m_X}{\mathrm{g}}}\,\mathrm{cm} = 10^{-2}\sqrt{\frac{m_X}{M_\odot}}\,\mathrm{pc.}^{14}$ The constraint on $\tilde{\alpha}_X$ is clearly consistent with our assumption that $\tilde{\alpha}_X \gg 1$ when $m_X \lesssim M_\odot$.

Now consider the indirect constraint on $\tilde{\alpha}$. If the DM and B fifth force charge to mass ratios are approximately independent of environment, then

$$\tilde{\alpha} \approx \sqrt{\tilde{\alpha}_n \tilde{\alpha}_X}.\tag{53}$$

Therefore the bullet cluster constraint plus a constraint on $\tilde{\alpha}_n$ lead to a constraint on $\tilde{\alpha}$:

$$\tilde{\alpha} < 5 \times 10^{-3} \left(\frac{\tilde{\alpha}_n^{\text{max}}}{10^{-11}} \right)^{1/2} \left(\frac{M_{\odot}}{m_X} \right)^{1/4} \left(\frac{v}{10^{-2}} \right) e^{2 \times 10^{-3} \sqrt{\frac{m_X}{M_{\odot}}} \frac{\text{pc}}{\lambda}}.$$
 (54)

 $^{^{14}}$ Conversely, the limit is very insensitive to λ as long as $\lambda\gg 10^{-2}\sqrt{\frac{m_X}{M_\odot}}\,\mathrm{pc}.$

We choose a fiducial value of 10^{-11} for $\tilde{\alpha}_n^{\text{max}}$ based on the MICROSCOPE limit [11, 12] but note that a more conservative limit based on inverse-square-law tests corresponds to $\tilde{\alpha}_n^{\text{max}} \sim 10^{-1}$ - 10^{-10} in the km to pc force range [1]. Furthermore, both the inverse square law and MICROSCOPE limits come from measuring accelerations on Earth and in our solar system—very different from the bullet cluster environment. A more conservative approach would not combine the limits at all. Furthermore, we note that the bullet cluster limit on DM sub-components weakens precipitously.

The limits in Eqs. 52 (red), 54 (purple), and 50 (blue) are represented in Fig. 4, along with the best constraint on $\tilde{\alpha}_n$, from Fig. 1 of [11] (green) for two force ranges at the boundaries of our range of interest. The inferred limit on $\tilde{\alpha}$ is just the geometric mean of the limits on $\tilde{\alpha}_X$ and $\tilde{\alpha}_n$.

V. SUMMARY AND CONCLUSIONS

We investigated probes of a long-range DM-baryon interaction. First, we derived limits on the interaction strength and range as functions of NS temperature and DM mass, density, and asymptotic speed distribution. This work extends the dark kinetic heating analysis of [28] to long-range forces and draws on the PBH gravitational tidal capture analysis of [56]. Fig. 2 shows our limit based on the coldest known NS. Next, extending the work in [27], we considered effects of a long-range fifth force on Doppler shifts of pulsar frequencies, and derived a limit based on the 11-yr NANOGrav PTA timing dataset, shown in Fig. 3. Finally, we considered *indirect* limits from weak equivalence principle tests and the bullet cluster, shown in Fig. 4. The three sets of constraints are shown together in Fig. 1. The indirect bullet cluster + WEP bound is stronger than the direct tidal heating and PTA bounds by an order of magnitude or more for all of the parameter space we considered. However, the tidal heating and PTA constraints are still interesting since they are direct phenomenological probes on DM-baryon interactions, independent of the microscopic origin of such a force. Moreover, if additional short-range interactions assist DM capture by NSs (allowing "maximal kinetic heating") or if only a subcomponent of DM interacts through the long-range fifth force, the kinetic heating and PTA limits dominate.

Imminent improvements on NS temperature and pulsar timing observations from, e.g., the James Webb Space Telescope [81] and Square Kilometer Array [82] will extend the

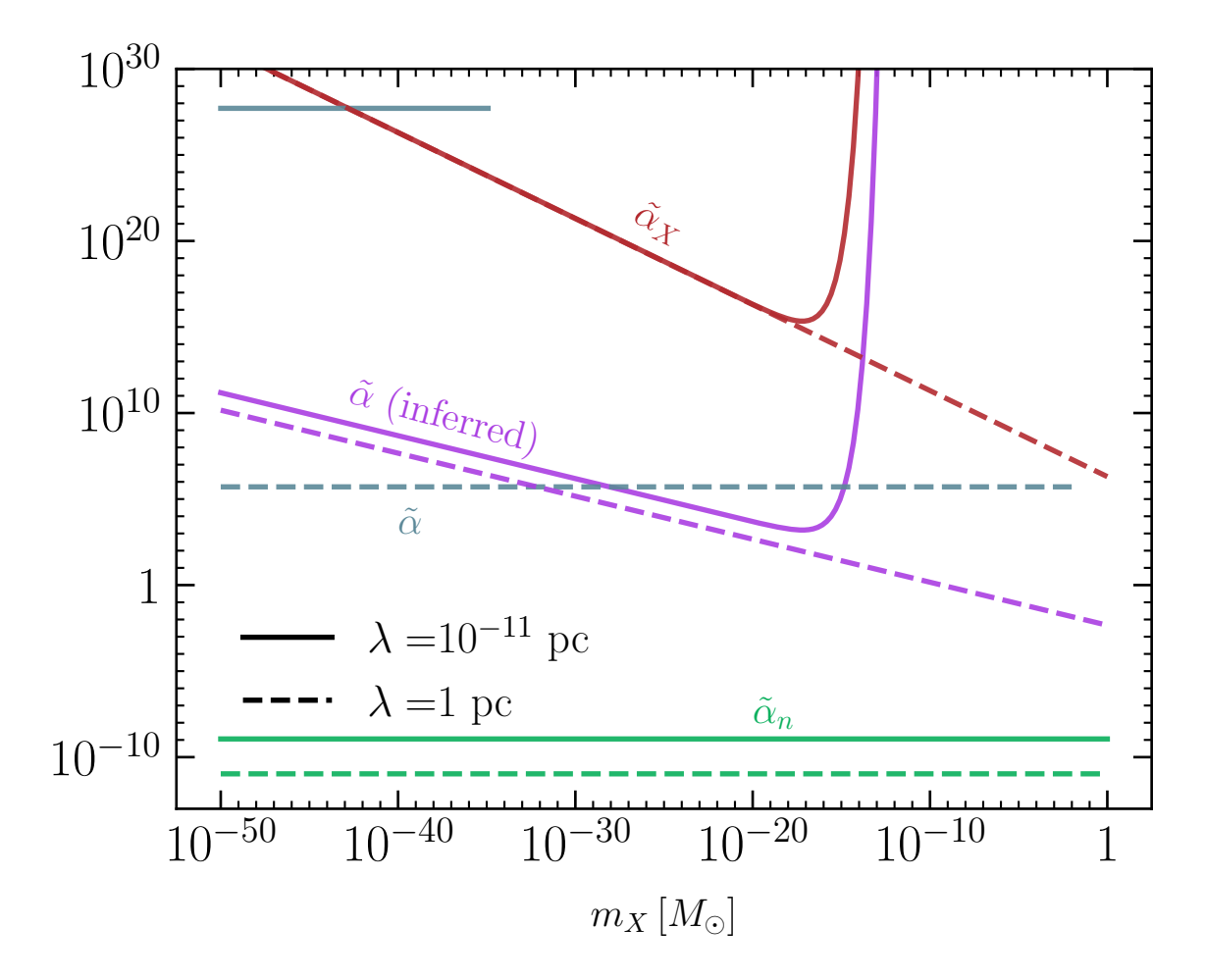


FIG. 4. Constraints on the fifth force to gravitational force strength ratios for baryonic matter self-interactions $(\tilde{\alpha}_n)$, DM-baryon interactions $(\tilde{\alpha})$, and DM self-interactions $(\tilde{\alpha}_X)$, from MICRO-SCOPE (Fig. 1 of [11]), weak equivalence principle tests constraining accelerations toward the galactic center (Eq. 50 and Table II), and the bullet cluster (Eq. 52), respectively, for force ranges at the extremes of those we consider. The inferred constraint on $\tilde{\alpha}$ (purple) is derived by combining the MICROSCOPE (green) and bullet cluster (red) limits, using $\tilde{\alpha}^{\text{max}} = \sqrt{\tilde{\alpha}_n^{\text{max}} \tilde{\alpha}_X^{\text{max}}}$ (Eq. 54). We have assumed that all of the DM in the Milky Way halo and in the bullet cluster takes the form of compact, effectively point-like states with approximately the same mass, m_X .

reach of NSs as probes of a long-range DM-baryon fifth force. In addition, the requirement for the NS cooling timescale to be smaller than the encounter timescale can be potentially relaxed by surveying a large population of NSs and searching for a fraction of them that are still cooling down after recent DM encounters [83]. On the other hand, higher than expected temperatures of isolated old NSs could be a sign of DM kinetic heating; if those

temperatures are higher than can be explained given kinetic heating through short-range interactions (c.f. [28] and Eq. 21 with $\tilde{\alpha}=0$), a long-range force could be part of the explanation. So could DM annihilation (see e.g. [84–88]) or other DM-induced exothermic processes (see e.g. [43, 89]). An unexpected NS temperature age dependence for old NSs in otherwise similar environments is another potential signature of a long-range force, since the heating rate can dramatically change once the effective charge of captured DM becomes comparable to that of the NS at birth. As discussed at the end of Sec. II, scalar-mediated interactions would lead to accelerated heating and vector-mediated to decelerated heating at late times. We leave detailed analyses of such possibilities for future work, should any observational hints arise.

ACKNOWLEDGMENTS

We thank Stephen Taylor and the NANOGrav collaboration for providing valuable guidance in deriving the PTA constraints. Some of this work was performed at the Aspen Center for Physics, which is supported by National Science Foundation grant PHY-1607611. MG's work was also supported by the National Science Foundation under Grant No. 1719780. The work of VL and KZ is supported by the DoE under contract DE-SC0011632, and by a Simons Investigator award. This work is also supported by the Walker Burke Institute for Theoretical Physics.

Appendix A: Classical Orbits and b_{max}

In this appendix we consider orbits of point-like DM about a static NS given both a gravitational and Yukawa force between them, as described in Sec. I. Our primary goal is to identify the impact parameters of orbits that intersect the NS, which requires finding the location of centrifugal barriers. The barriers can occur at radii $r \gtrsim \lambda$ where the fifth force is starting to turn on, and at radii much smaller than the force range, where general and special relativity can be relevant. We begin with a reminder of the gravity-only case and then generalize to include the Yukawa interaction.

The general relativistic expression of energy conservation given a spherically symmetric star of mass M and a much lighter orbiting body of mass m comes from the constraint

 $p_{\mu}p^{\mu}=-m^2$. Employing the Schwarzschild metric and coordinates, $p_t=g_{tt}m\frac{dt}{d\tau}=-E=-m\gamma$ and $p_{\phi}=g_{\phi\phi}m\frac{d\phi}{d\tau}=L=\gamma mbv$ are conserved quantities along geodesics, where v is the asymptotic DM speed, $\gamma=1/\sqrt{1-v^2}$, and b is the impact parameter. With these identifications the constraint reads,

$$\left(\frac{dr}{d\tau}\right)^2 = \frac{E^2}{m^2} - \left(\frac{(L/m)^2}{r^2} + 1\right) \left(1 - \frac{2GM}{r}\right). \tag{A1}$$

Given a large enough impact parameter, DM streaming in from infinity with asymptotic speed v hits a centrifugal barrier, where $\frac{dr}{d\tau} \to 0$.

Given an additional attractive Yukawa interaction, the four-momentum constraint is the same, but $E \to E - V_{\text{Yuk}}$. So orbits obey¹⁵

$$\left(\frac{dr}{d\tau}\right)^2 = \left(\frac{E - V_{\text{eff},+}}{m}\right) \left(\frac{E - V_{\text{eff},-}}{m}\right) \tag{A2}$$

with¹⁶

$$\frac{V_{\text{eff},\pm}}{m} = -\frac{GM\tilde{\alpha}e^{-r/\lambda}}{r} \pm \sqrt{\left(1 - \frac{2GM}{r}\right)\left(\frac{(L/m)^2}{r^2} + 1\right)}.$$
 (A3)

The turning points, r_{\min} , of unbound orbits—i.e. centrifugal barriers—occur at the maximum radial coordinate for which $V_{\text{eff},+} = E$. Solving the condition for the impact parameter, b, yields,

$$b(r_{\min}) = r_{\min} \sqrt{\frac{1 + \frac{2GM}{r_{\min}\gamma^2 v^2} \left(1 + \tilde{\alpha}e^{-r_{\min}/\lambda}\right) + \left(\frac{GM}{r_{\min}\gamma v}\tilde{\alpha}e^{-r_{\min}/\lambda}\right)^2}{\left(1 - \frac{2GM}{r_{\min}}\right)}}.$$
 (A4)

DM focused through gravity alone breaches a NS surface iff $b < b(R)|_{\tilde{\alpha} \to 0} = R\sqrt{1 + \frac{2GM/Rv^2}{1-2GM/R}} \approx \sqrt{\frac{2GMR/v^2}{1-2GM/R}}$.

For large $\tilde{\alpha}$, the exponential turn-on of the fifth force can lead to an additional partial centrifugal barrier at $r > \lambda$, and the peak of the inner centrifugal barrier near the Schwarzschild radius moves to larger radial coordinates. These behaviors are demonstrated in Fig. 5, which shows examples of $V_{\rm eff, +}$ and E assuming $v = 10^{-3}$ for $\lambda = 10^{-11}$ pc. When $\tilde{\alpha} = 20$ (orange), the centrifugal barrier appears first in the inner region where $r < \lambda$. When $\tilde{\alpha} = 50$ (purple), the centrifugal barrier appears in the outer region where $r > 2\lambda$. In these examples, DM $\overline{^{15}}$ The NS's fifth force charge could non-negligibly affect the general relativistic lapse function when $\frac{G\alpha_nQ_{\rm NS}^2}{R^2} = \tilde{\alpha}_n \left(\left(\frac{Q}{M/m_n}\right)_{\rm NS}\frac{GM}{R}\right)^2 \gtrsim 0.1$. So a consistency requirement is $\sqrt{\tilde{\alpha}_n}\left(\frac{Q}{M/m_n}\right)_{\rm NS} \ll 1$. Since equivalence principle measurements restrict $\tilde{\alpha}_n \lesssim 10^{-11}$ - 10^{-9} for the force ranges we examine, the condition easily holds when baryonic charge (and not captured DM charge) dominates the total NS charge. $\frac{16}{\rm C.f.}$ [90].

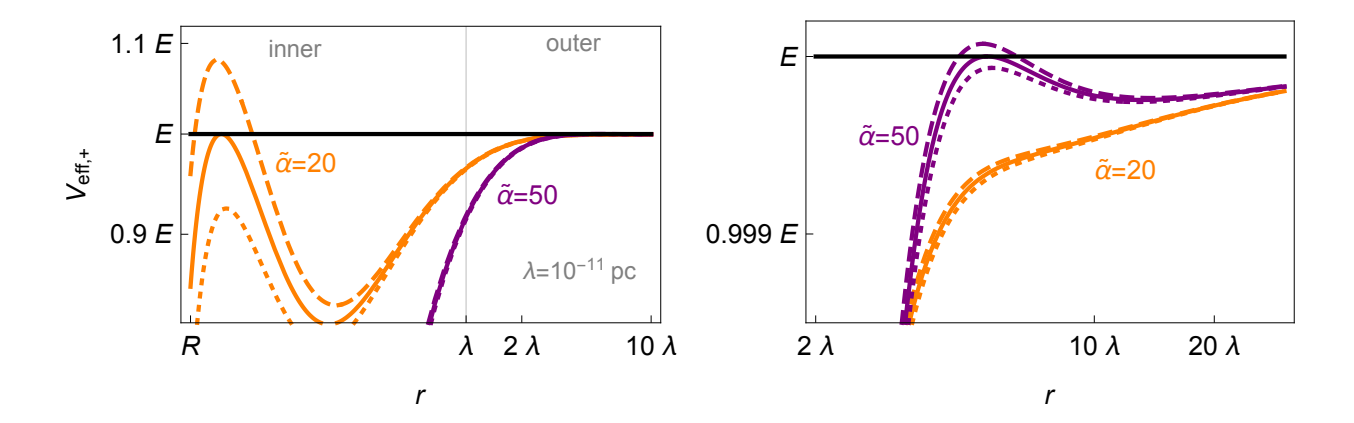


FIG. 5. $V_{\rm eff,+}$ as a function of DM radial coordinate when $b=b_{\rm max}$ (solid) and $b=10^{\pm0.01}b_{\rm max}$ (dashed/dotted), with $\lambda=10^{-11}\,{\rm pc},\ v=10^{-3},\ {\rm and}\ \tilde{\alpha}=20$ (orange) or $\tilde{\alpha}=50$ (purple). The right-hand plot shows only the outer region, with the vertical (logarithmic) scale magnified. In this example, the inner barrier determines $b_{\rm max}$ for $\tilde{\alpha}=20$ while the outer barrier determines $b_{\rm max}$ for $\tilde{\alpha}=50$. C.f. Fig. 6.

orbits either hit a centrifugal barrier at r > R or they intersect the neutron surface when $\frac{dr}{d\tau} > 0$; there are no orbits that just barely touch the NS surface.

The solid lines in Fig. 5 correspond to conserved angular momentum $L = \gamma m b_{\text{max}} v$. For large $\tilde{\alpha}$, as can be seen in the figure, b_{max} and the coordinate of the barrier's peak, r_{b} , are the solutions to

$$V'_{\text{eff, +}}(r_{\text{b}})|_{L=\gamma mb_{\text{max}}v} = 0, \qquad V_{\text{eff, +}}(r_{\text{b}})|_{L=\gamma mb_{\text{max}}v} = \gamma m.$$
 (A5)

For very large $\tilde{\alpha}$ there are two solutions, corresponding to the inner and outer barriers, respectively. The maximum impact parameter of DM that intersects the NS is the solution with smallest b_{max} .

Using $v^2 \ll \frac{GM}{R} \ll 1$ and $\lambda \gg R$, we find that a very good analytic approximation for b_{max} is given by the minimum of

$$b_{\text{max, inner}} \approx \frac{R}{v} \sqrt{\frac{\frac{2GM}{R} \left(1 + \tilde{\alpha}e^{-R/\lambda}\right) + \left(\frac{GM}{R}\tilde{\alpha}e^{-R/\lambda}\right)^2}{\left(1 - \frac{2GM}{R}\right)}}$$
(A6)

and

$$b_{\text{max, outer}} \approx \sqrt{\lambda x \left(\frac{2GM}{v^2} + \lambda x\right)} \text{ with } x \approx \log\left(\frac{\tilde{\alpha}}{\frac{\lambda v^2}{GM} + \frac{1}{\log \tilde{\alpha}}}\right) \gtrsim 2 + \log 2,$$
 (A7)

$$b_{\text{max}} = \min \left(b_{\text{max, inner}}, b_{\text{max, outer}} \right). \tag{A8}$$

Fig. 6 shows our analytic approximation in Eq. A8 (color) alongside numerical solutions to Eq. A5 (black)¹⁷ as a function of $\tilde{\alpha}$ for three choices of force range, λ , assuming $v \sim 10^{-3}$, $R = 10 \,\mathrm{km}$, and $\frac{GM}{R} = 0.2$. The inner barrier controls b_{max} at small $\tilde{\alpha}$. For $\tilde{\alpha} \gg 1$, b_{max} grows in proportion to $\tilde{\alpha}$ until it is cut to logarithmic growth because of the outer centrifugal barrier at radial distances greater than λ .

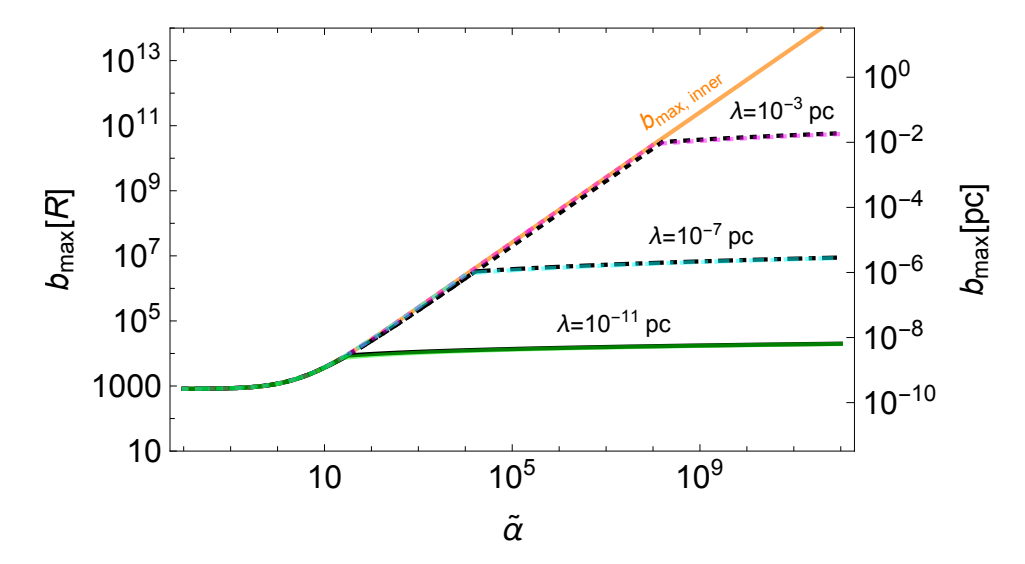


FIG. 6. Maximum impact parameter for which DM with asymptotic speed $v \sim 10^{-3}$ intersects a NS with circumferential radius R, assuming $\frac{GM}{R} = 0.2$, as a function of $\tilde{\alpha}$. The quoted λ values and right-hand scale assume $R = 10 \, \mathrm{km}$. The black lines show (more exact) numerical results while the colored lines show our analytic approximation in Eq. A8, which agrees with the numerical results to within better than a factor of 2 in the entire range. The kink in the b_{max} curves correspond to the point where the outer centrifugal barrier at $r > \lambda$ occurs at smaller b than the inner barrier closer to $r \sim R$. C.f. Fig. 5.

We end this appendix with a few comments on our analytic approximation and the behavior of b_{max} . Eq. A6 is the impact parameter for which the effective potential equals E at the NS surface in the $v \ll 1$ limit—i.e. b(R) from Eq. A4. It is only a slight overestimate of the impact parameter for which the inner centrifugal barrier peaks at E (c.f. Fig. 5),

When $\frac{GM}{R} = 0.2$ and $\lambda \gg R$, $r_{\rm p} \lesssim R$ when $\tilde{\alpha} \lesssim 6$, and $b_{\rm max}$ is given exactly by Eq. A6. The exact cutoff at small $\tilde{\alpha}$ depends somewhat sensitively on $\frac{GM}{R}$.

and it is exact in the limit $\tilde{\alpha} \to 0$. In the opposite limit and when $\lambda \gg R$, $b_{\max, \text{ inner}} \approx \frac{GM}{v}\tilde{\alpha}$; the effective radius of the NS is approximately the geometric mean of the Coulomb classical and circular radii $(GM\tilde{\alpha} \text{ and } \frac{GM\tilde{\alpha}}{v^2}, \text{ respectively})$. Eq. A7 comes from analyzing the effective potential in the $\frac{GM}{r}$, $\frac{(L/m)^2}{r^2} \ll 1$ limit (the nonrelativistic limit), and $r_p \approx \lambda x$. For $x \lesssim 2$, the outer barrier does not exist. When the Yukawa force is much smaller than the gravitational force at the gravitational circular radius, $\tilde{\alpha}e^{-GM/v^2\lambda} \ll 1$, gravity is important in determining $b_{\max, \text{ outer}}$, and $b_{\max, \text{ outer}} \to \frac{1}{v}\sqrt{2\lambda GM\log(\tilde{\alpha}\log\tilde{\alpha})}$. In the opposite extreme, when $\tilde{\alpha}e^{-GM/v^2\lambda} > 1$, gravity is unimportant in determining the location of the barrier, and $b_{\max, \text{ outer}} \to \lambda\log\left(\frac{\tilde{\alpha}GM}{\lambda v^2}\right)$. This latter case is the only one where $b_{\max}v$ evolves appreciably as a function of v; in all other limits discussed, $b_{\max}v$ is essentially constant. When computing averages over the asymptotic DM velocity distribution, we use the fact that bv is nearly constant or—in the limit just discussed—mildly increasing (less than linearly) as a function of v.

Appendix B: Timescale for heating once captured

In this appendix we estimate the period of the first obit after DM is captured by depositing energy $\Delta E_{\rm graze}$ during a transit of a NS. Our approach is inspired by that in [56]. As long as the apastron of this orbit, $r_{\rm max}$, is large so that $\tilde{\alpha} \frac{GM}{r_{\rm max}} e^{-r_{\rm max}/\lambda}$, $\frac{GM}{r_{\rm max}} \ll 1$, a non-relativistic treatment yields a good estimate because then the DM is non-relativistic on parts of its trajectory near the apastron, where it spends the majority of its time. We proceed with a non-relativistic analysis.

The apastron is related to the DM's conserved non-relativistic energy, E, and orbital angular momentum magnitude, L, through

$$E = -\frac{GMm_X}{r_{\text{max}}} \left(1 + \tilde{\alpha}e^{-r_{\text{max}}/\lambda}\right) + \frac{1}{2} \frac{L^2}{m_X r_{\text{max}}^2}.$$
 (B1)

And the period of an orbit with apastron r_{max} and periastron r_{min} is

$$\Delta t = 2 \int_{r_{\min}}^{r_{\max}} \frac{dr}{\dot{r}} = 2 \int_{r_{\min}}^{r_{\max}} \left(\frac{2E}{m_X} + \frac{2GM}{r} \left(1 + \tilde{\alpha}e^{-r/\lambda} \right) - \frac{(L/m_X)^2}{r^2} \right)^{-1/2} dr.$$
 (B2)

When $v \ll 1$, we expect $(L/m) \approx bv$ to be nearly independent of v for orbits that sweep near the NS surface because the kinetic energy at closest approach is essentially independent of v; it is instead dominated by the fifth force and gravitational potential energy loss.

Assuming orbital angular momentum doesn't increase upon capture, $L_{\text{closed orbit}} \leq m_X b_{\text{max}} v$, and the orbital angular momentum term negligibly affects the period of orbits with $r_{\text{max}} \gg R$, which are the orbits with the largest contribution to the total energy deposit timescale, we get

$$\Delta t \approx 2 \int_0^{r_{\text{max}}} \left(\frac{2GM(1 + \tilde{\alpha}e^{-r/\lambda})}{r} - \frac{2GM(1 + \tilde{\alpha}e^{-r_{\text{max}}/\lambda})}{r_{\text{max}}} \right)^{-1/2} dr.$$
 (B3)

The above equation is the period of a maximally eccentric orbit. It reduces to Kepler's third law, $\Delta t = 2\pi \frac{a^{3/2}}{\sqrt{GM}}$ for a maximally eccentric orbit, where $a = r_{\text{max}}/2$, when the ratio of the fifth force to the gravitational force at the apastron is very small, $\tilde{\alpha}(1 + \frac{r_{\text{max}}}{\lambda})e^{-r_{\text{max}}/\lambda} \ll 1$. To extremely good accuracy when the force ratio at the apastron is either very small or very large, we find the integral can be approximated as

$$\Delta t \approx \frac{\Delta t_{\circ}(r_{\text{max}})}{2\sqrt{2}} = \frac{\pi}{\sqrt{2}} \frac{r_{\text{max}}^{3/2} / \sqrt{GM}}{\sqrt{1 + \tilde{\alpha} \left(1 + \frac{r_{\text{max}}}{\lambda}\right) e^{-r_{\text{max}}/\lambda}}}$$
(B4)

where $\Delta t_{\rm o}$ is the period of a circular orbit with radius $r_{\rm max}$. Eq. B4 is an overestimate. The overestimate is most significant when the force ratio at the apastron is comparable to 1 and $\tilde{\alpha}$ is large, but it comes within a factor of 4 as long as $\tilde{\alpha} \lesssim 10^{30}$.

The apastron of the orbit after the first encounter, $r_{\text{max},1}$, is given by the solution to

$$\frac{1}{2}m_X v^2 - \Delta E_{\text{graze}} = -\frac{GMm_X}{r_{\text{max},1}} \left(1 + \tilde{\alpha} e^{-r_{\text{max},1}/\lambda} \right) + \frac{m_X}{2} \frac{(L_1/m_X)^2}{r_{\text{max},1}^2}.$$
 (B5)

A good estimate of the period of the first orbit after capture, Δt_1 , is given by Eq. B4 evaluated at $r_{\text{max}} = r_{\text{max},1}$ determined by Eq. B5 with $L_1 = 0$ (a maximally eccentric orbit). We note that $r_{\text{max},1}$ is an increasing function of v and $r_{\text{max},1}(v) < r_{\text{max},1}(0)/(1-v^2/v_{\text{max}}^2)$ so that $\Delta t(v) \lesssim \frac{\Delta t(0)}{(1-v^2/v_{\text{cap}}^2)^{3/2}}$. For asymptotic speeds up to about $0.8 v_{\text{cap}}$, $\Delta t_1(v) \approx \Delta t_1(0)$ is a good estimate; the period rapidly asymptotes to infinity thereafter, as $v \to v_{\text{cap}}$.

Altogether, we have,

$$\Delta t_1(0) \approx GM \frac{\pi}{\sqrt{2}} \left(\frac{m_X}{\Delta E_{\text{graze}}} \right)^{3/2} \frac{\left(1 + \tilde{\alpha} e^{-r_{\text{max},1}/\lambda} \right)^{3/2}}{\sqrt{1 + \tilde{\alpha} \left(1 + \frac{r_{\text{max},1}}{\lambda} \right) e^{-r_{\text{max},1}/\lambda}}}$$
(B6)

where we redefined $r_{\text{max},1}$ to be defined through Eq. B5 with $v = 0, L_1 = 0$:

$$\Delta E_{\text{graze}} = \frac{GMm_X}{r_{\text{max, 1}}} (1 + \tilde{\alpha}e^{-r_{\text{max, 1}}/\lambda}). \tag{B7}$$

When $r_{\text{max},1} \gg \lambda$ and $\frac{r_{\text{max},1}}{\lambda} \tilde{\alpha} e^{-r_{\text{max},1}/\lambda} \ll 1$, the period of the first orbit after capture is approximately $\Delta t_1 \approx GM \frac{\pi}{\sqrt{2}} \left(\frac{m_X}{\Delta E_{\text{graze}}}\right)^{3/2}$. When $r_{\text{max},1} \sim \frac{GM m_X (1+\tilde{\alpha})}{\Delta E_{\text{graze}}} \ll \lambda$, $\Delta t_1 \approx GM \frac{\pi}{\sqrt{2}} \left(\frac{m_X}{\Delta E_{\text{graze}}}\right)^{3/2} (1+\tilde{\alpha})$.

The timescale is the limiting factor in the tidal heating rate when $\Delta t_1 \gtrsim t_{\rm NS}$. From Eq. B4, $t_{\rm max,1} > \left(\frac{\sqrt{2GM}}{\pi}\Delta t_1(0)\right)^{2/3}$ so $\Delta t_1 \gtrsim t_{\rm NS}$ requires $t_{\rm max} \gtrsim \left(t_{\rm NS}\sqrt{GM}\right)^{2/3} \sim 10\,{\rm pc}\left(\frac{t_{\rm NS}}{\rm Gyr}\right)^{2/3}$. For $\lambda \ll \left(t_{\rm NS}\sqrt{GM}\right)^{2/3}$ and $\tilde{\alpha} < \frac{\lambda}{\left(t_{\rm NS}\sqrt{GM}\right)^{2/3}}e^{\left(t_{\rm NS}\sqrt{GM}\right)^{2/3}/\lambda}$, we see $\Delta t_1 = t_{\rm NS}$ corresponds to the contour $\Delta t_1 = GM\frac{\pi}{\sqrt{2}}\left(\frac{m_X}{\Delta E_{\rm graze}}\right)^{3/2} = t_{\rm NS}$.

Appendix C: Pulsar Glitches

In principle DM can transfer both energy and angular momentum to pulsars. At most, DM can transfer its entire angular momentum, $m_X bv$, during a close-range interaction. This would cause a typical shift in the pulsar frequency—a glitch—of at most

$$\Delta \nu \approx \frac{|\Delta L_{\rm NS}|}{I_{\rm NS}} \approx \frac{m_X \langle b_{\rm max} v \rangle}{\frac{2}{5} M R^2} \approx 10^5 \left(\frac{m_X}{M}\right) \left(\frac{\langle b_{\rm max} v \rangle}{R}\right) \left(\frac{10 \, {\rm km}}{R}\right) {\rm Hz}. \tag{C1}$$

Meanwhile, the DM glitch rate per NS is at most the DM flux, given by,

$$\dot{N}_{\rm glitch} \lesssim \frac{\rho_X}{m_X} \pi \langle b_{\rm max}^2 v \rangle \sim \frac{10^{-24}}{\rm yr} \frac{R^2}{(10\,{\rm km})^2} \frac{\rho_X}{0.4\,{\rm GeV/\,cm}^3} \frac{1.4M_{\odot}}{M} \frac{10^{-3}}{v_p} \left(\frac{\langle b_{\rm max}^2 v \rangle v_p}{R^2}\right) \frac{M}{m_X}.$$
 (C2)

Consider $\Delta \nu \sim 10^{-9} {\rm Hz}$ as a benchmark.¹⁹ Given gravity only, $\langle b_{\rm max} v \rangle / R \sim 1$, requiring $m_X/M \gtrsim 10^{-14}$ for a glitch of order $10^{-9} {\rm Hz}$ or greater, and the rate for such glitches is order $\dot{N}_{\rm glitch} \sim \frac{10^{-10}}{{\rm yr}}$ or less for the fiducial parameters in Eq. C2.

However, the presence of a DM-NS fifth force with range greater than order a thousand kilometers opens up the possibility for larger $b_{\rm max}$; thus smaller m_X could cause detectable glitches at greater rates than in the gravity-only case just discussed. Given maximal kinetic heating, the coldest observed NS constrains $\tilde{\alpha} \lesssim 10^2$ for $\lambda \gtrsim 10^{-10}$ pc (see Eq. 33), corresponding to $\frac{\langle b_{\rm max} v \rangle}{R} \lesssim \frac{GM}{R} 10^2 \sim 20$. To get typical glitches of order 10^{-9} Hz or greater, one would require $\frac{m_X}{M} \gtrsim 10^{-15}$ and thus a glitch rate less than about 10^{-6} per NS per year.

To conclude, in principle, a DM-baryon fifth force may have given rise to an interesting

See Ref. [94] for a discussion of thresholds.

DM-induced pulsar glitch phenomenon, but kinetic heating limits rule this out.

[1] E. Adelberger, B. Heckel, and A. Nelson, Tests of the gravitational inverse-square law, Annual Review of Nuclear and Particle Science 53, 77 (2003).

- [2] E. Hardy, R. Lasenby, J. March-Russell, and S. M. West, Big Bang Synthesis of Nuclear Dark Matter, JHEP 06, 011, arXiv:1411.3739 [hep-ph].
- [3] G. Krnjaic and K. Sigurdson, Big Bang Darkleosynthesis, Phys. Lett. B **751**, 464 (2015), arXiv:1406.1171 [hep-ph].
- [4] W. Detmold, M. McCullough, and A. Pochinsky, Dark Nuclei I: Cosmology and Indirect Detection, Phys. Rev. D **90**, 115013 (2014), arXiv:1406.2276 [hep-ph].
- [5] M. B. Wise and Y. Zhang, Stable Bound States of Asymmetric Dark Matter, Phys. Rev. D
 90, 055030 (2014), [Erratum: Phys.Rev.D 91, 039907 (2015)], arXiv:1407.4121 [hep-ph].
- [6] M. I. Gresham, H. K. Lou, and K. M. Zurek, Early Universe synthesis of asymmetric dark matter nuggets, Phys. Rev. D 97, 036003 (2018), arXiv:1707.02316 [hep-ph].
- [7] M. I. Gresham, H. K. Lou, and K. M. Zurek, Nuclear Structure of Bound States of Asymmetric Dark Matter, Phys. Rev. D 96, 096012 (2017), arXiv:1707.02313 [hep-ph].
- [8] M. I. Gresham, H. K. Lou, and K. M. Zurek, Astrophysical Signatures of Asymmetric Dark Matter Bound States, Phys. Rev. D 98, 096001 (2018), arXiv:1805.04512 [hep-ph].
- [9] M. I. Gresham and K. M. Zurek, Asymmetric Dark Stars and Neutron Star Stability, Phys. Rev. D 99, 083008 (2019), arXiv:1809.08254 [astro-ph.CO].
- [10] D. Kim, Y. Kim, Y. K. Semertzidis, Y. C. Shin, and W. Yin, Cosmic axion force, Physical Review D 104, 10.1103/physrevd.104.095010 (2021).
- [11] J. Bergé, P. Brax, G. Métris, M. Pernot-Borràs, P. Touboul, and J.-P. Uzan, MICROSCOPE Mission: First Constraints on the Violation of the Weak Equivalence Principle by a Light Scalar Dilaton, Phys. Rev. Lett. 120, 141101 (2018), arXiv:1712.00483 [gr-qc].
- [12] P. Fayet, MICROSCOPE limits on the strength of a new force, with comparisons to gravity and electromagnetism, Phys. Rev. D **99**, 055043 (2019), arXiv:1809.04991 [hep-ph].
- [13] D. N. Spergel and P. J. Steinhardt, Observational evidence for selfinteracting cold dark matter, Phys. Rev. Lett. 84, 3760 (2000), arXiv:astro-ph/9909386.
- [14] F. Kahlhoefer, K. Schmidt-Hoberg, M. T. Frandsen, and S. Sarkar, Colliding clusters and

- dark matter self-interactions, Mon. Not. Roy. Astron. Soc. 437, 2865 (2014), arXiv:1308.3419 [astro-ph.CO].
- [15] A. Coskuner, D. M. Grabowska, S. Knapen, and K. M. Zurek, Direct Detection of Bound States of Asymmetric Dark Matter, Phys. Rev. D 100, 035025 (2019), arXiv:1812.07573 [hep-ph].
- [16] E. R. Siegel, M. P. Hertzberg, and J. N. Fry, Probing dark matter substructure with pulsar timing, Monthly Notices of the Royal Astronomical Society 382, 879 (2007).
- [17] N. Seto and A. Cooray, Searching for primordial black hole dark matter with pulsar timing arrays, The Astrophysical Journal 659, L33 (2007).
- [18] K. Kashiyama and N. Seto, Enhanced exploration for primordial black holes using pulsar timing arrays, Monthly Notices of the Royal Astronomical Society **426**, 1369 (2012).
- [19] H. A. Clark, G. F. Lewis, and P. Scott, Investigating dark matter substructure with pulsar timing – i. constraints on ultracompact minihaloes, Monthly Notices of the Royal Astronomical Society 456, 1394 (2015).
- [20] H. A. Clark, G. F. Lewis, and P. Scott, Investigating dark matter substructure with pulsar timing – II. improved limits on small-scale cosmology, Monthly Notices of the Royal Astronomical Society 456, 1402 (2015).
- [21] K. Schutz and A. Liu, Pulsar timing can constrain primordial black holes in the LIGO mass window, Physical Review D **95**, 10.1103/physrevd.95.023002 (2017).
- [22] K. Kashiyama and M. Oguri, Detectability of small-scale dark matter clumps with pulsar timing arrays (2018).
- [23] S. Baghram, N. Afshordi, and K. M. Zurek, Prospects for Detecting Dark Matter Halo Substructure with Pulsar Timing, Phys. Rev. D 84, 043511 (2011), arXiv:1101.5487 [astro-ph.CO].
- [24] J. A. Dror, H. Ramani, T. Trickle, and K. M. Zurek, Pulsar Timing Probes of Primordial Black Holes and Subhalos, Phys. Rev. D 100, 023003 (2019), arXiv:1901.04490 [astro-ph.CO].
- [25] H. Ramani, T. Trickle, and K. M. Zurek, Observability of Dark Matter Substructure with Pulsar Timing Correlations, JCAP 12, 033, arXiv:2005.03030 [astro-ph.CO].
- [26] V. S. H. Lee, A. Mitridate, T. Trickle, and K. M. Zurek, Probing small-scale power spectra with pulsar timing arrays, Journal of High Energy Physics 2021, 10.1007/jhep06(2021)028 (2021).
- [27] V. S. Lee, S. R. Taylor, T. Trickle, and K. M. Zurek, Bayesian forecasts for dark matter

- substructure searches with mock pulsar timing data, Journal of Cosmology and Astroparticle Physics **2021** (08), 025.
- [28] M. Baryakhtar, J. Bramante, S. W. Li, T. Linden, and N. Raj, Dark Kinetic Heating of Neutron Stars and An Infrared Window On WIMPs, SIMPs, and Pure Higgsinos, Phys. Rev. Lett. 119, 131801 (2017), arXiv:1704.01577 [hep-ph].
- [29] N. Raj, P. Tanedo, and H.-B. Yu, Neutron stars at the dark matter direct detection frontier, Phys. Rev. D 97, 043006 (2018), arXiv:1707.09442 [hep-ph].
- [30] R. Garani, Y. Genolini, and T. Hambye, New Analysis of Neutron Star Constraints on Asymmetric Dark Matter, JCAP **05**, 035, arXiv:1812.08773 [hep-ph].
- [31] N. F. Bell, G. Busoni, and S. Robles, Heating up Neutron Stars with Inelastic Dark Matter, JCAP **09**, 018, arXiv:1807.02840 [hep-ph].
- [32] N. F. Bell, G. Busoni, and S. Robles, Capture of Leptophilic Dark Matter in Neutron Stars, JCAP **06**, 054, arXiv:1904.09803 [hep-ph].
- [33] R. Garani and J. Heeck, Dark matter interactions with muons in neutron stars, Phys. Rev. D 100, 035039 (2019), arXiv:1906.10145 [hep-ph].
- [34] J. F. Acevedo, J. Bramante, R. K. Leane, and N. Raj, Warming Nuclear Pasta with Dark Matter: Kinetic and Annihilation Heating of Neutron Star Crusts, JCAP 03, 038, arXiv:1911.06334 [hep-ph].
- [35] A. Joglekar, N. Raj, P. Tanedo, and H.-B. Yu, Relativistic capture of dark matter by electrons in neutron stars, Phys. Lett. B, 135767 (2020), arXiv:1911.13293 [hep-ph].
- [36] B. Dasgupta, A. Gupta, and A. Ray, Dark matter capture in celestial objects: light mediators, self-interactions, and complementarity with direct detection, JCAP 10, 023, arXiv:2006.10773 [hep-ph].
- [37] W.-Y. Keung, D. Marfatia, and P.-Y. Tseng, Heating neutron stars with GeV dark matter, JHEP 07, 181, arXiv:2001.09140 [hep-ph].
- [38] A. Joglekar, N. Raj, P. Tanedo, and H.-B. Yu, Dark kinetic heating of neutron stars from contact interactions with relativistic targets, Phys. Rev. D 102, 123002 (2020), arXiv:2004.09539 [hep-ph].
- [39] N. F. Bell, G. Busoni, T. F. Motta, S. Robles, A. W. Thomas, and M. Virgato, Nucleon Structure and Strong Interactions in Dark Matter Capture in Neutron Stars, Phys. Rev. Lett. 127, 111803 (2021), arXiv:2012.08918 [hep-ph].

- [40] N. F. Bell, G. Busoni, S. Robles, and M. Virgato, Improved Treatment of Dark Matter Capture in Neutron Stars II: Leptonic Targets, JCAP 03, 086, arXiv:2010.13257 [hep-ph].
- [41] R. Garani, A. Gupta, and N. Raj, Observing the thermalization of dark matter in neutron stars, Phys. Rev. D **103**, 043019 (2021), arXiv:2009.10728 [hep-ph].
- [42] T. N. Maity and F. S. Queiroz, Detecting bosonic dark matter with neutron stars, Phys. Rev. D 104, 083019 (2021), arXiv:2104.02700 [hep-ph].
- [43] D. McKeen, M. Pospelov, and N. Raj, Neutron Star Internal Heating Constraints on Mirror Matter, Phys. Rev. Lett. 127, 061805 (2021), arXiv:2105.09951 [hep-ph].
- [44] C. Ilie and C. Levy, Multicomponent multiscatter capture of dark matter, Phys. Rev. D 104, 083033 (2021), arXiv:2105.09765 [astro-ph.CO].
- [45] C. Ilie and J. Paulin, Analytic Approximations for the Velocity Suppression of Dark Matter Capture, Astrophys. J. **932**, 46 (2022), arXiv:2107.00675 [astro-ph.CO].
- [46] N. F. Bell, G. Busoni, S. Robles, and M. Virgato, Improved Treatment of Dark Matter Capture in Neutron Stars, JCAP 09, 028, arXiv:2004.14888 [hep-ph].
- [47] J. Bramante, B. J. Kavanagh, and N. Raj, Scattering Searches for Dark Matter in Subhalos: Neutron Stars, Cosmic Rays, and Old Rocks, Phys. Rev. Lett. 128, 231801 (2022), arXiv:2109.04582 [hep-ph].
- [48] S. Guillot, G. G. Pavlov, C. Reyes, A. Reisenegger, L. E. Rodriguez, B. Rangelov, and O. Kargaltsev, Hubble space telescope nondetection of psr j2144–3933: The coldest known neutron star, The Astrophysical Journal 874, 175 (2019).
- [49] Z. Arzoumanian, A. Brazier, S. Burke-Spolaor, S. Chamberlin, S. Chatterjee, B. Christy, J. M. Cordes, N. J. Cornish, F. Crawford, H. T. Cromartie, K. Crowter, M. E. DeCesar, P. B. Demorest, T. Dolch, J. A. Ellis, R. D. Ferdman, E. C. Ferrara, E. Fonseca, N. Garver-Daniels, P. A. Gentile, D. Halmrast, E. A. Huerta, F. A. Jenet, C. Jessup, G. Jones, M. L. Jones, D. L. Kaplan, M. T. Lam, T. J. W. Lazio, L. Levin, A. Lommen, D. R. Lorimer, J. Luo, R. S. Lynch, D. Madison, A. M. Matthews, M. A. McLaughlin, S. T. McWilliams, C. Mingarelli, C. Ng, D. J. Nice, T. T. Pennucci, S. M. Ransom, P. S. Ray, X. Siemens, J. Simon, R. Spiewak, I. H. Stairs, D. R. Stinebring, K. Stovall, J. K. Swiggum, S. R. Taylor, M. Vallisneri, R. van Haasteren, S. J. Vigeland, and W. Z. and, The NANOGrav 11-year data set: High-precision timing of 45 millisecond pulsars, The Astrophysical Journal Supplement Series 235, 37 (2018).
- [50] Z. Arzoumanian, P. T. Baker, A. Brazier, S. Burke-Spolaor, S. J. Chamberlin, S. Chatter-

- jee, B. Christy, J. M. Cordes, N. J. Cornish, F. Crawford, H. T. Cromartie, K. Crowter, M. DeCesar, P. B. Demorest, T. Dolch, J. A. Ellis, R. D. Ferdman, E. Ferrara, W. M. Folkner, E. Fonseca, N. Garver-Daniels, P. A. Gentile, R. Haas, J. S. Hazboun, E. A. Huerta, K. Islo, G. Jones, M. L. Jones, D. L. Kaplan, V. M. Kaspi, M. T. Lam, T. J. W. Lazio, L. Levin, A. N. Lommen, D. R. Lorimer, J. Luo, R. S. Lynch, D. R. Madison, M. A. McLaughlin, S. T. McWilliams, C. M. F. Mingarelli, C. Ng, D. J. Nice, R. S. Park, T. T. Pennucci, N. S. Pol, S. M. Ransom, P. S. Ray, A. Rasskazov, X. Siemens, J. Simon, R. Spiewak, I. H. Stairs, D. R. Stinebring, K. Stovall, J. Swiggum, S. R. Taylor, M. Vallisneri, R. van Haasteren, S. Vigeland, and W. W. Z. and, The NANOGrav 11 year data set: Pulsar-timing constraints on the stochastic gravitational-wave background, The Astrophysical Journal 859, 47 (2018).
- [51] A. Brazier, S. Chatterjee, T. Cohen, J. M. Cordes, M. E. DeCesar, P. B. Demorest, J. S. Hazboun, M. T. Lam, R. S. Lynch, M. A. McLaughlin, S. M. Ransom, X. Siemens, S. R. Taylor, and S. J. Vigeland, The nanograv program for gravitational waves and fundamental physics (2019), arXiv:1908.05356 [astro-ph.IM].
- [52] H. Davoudiasl, Dark matter repulsion could thwart direct detection, Phys. Rev. D 96, 095019(2017), arXiv:1705.00028 [hep-ph].
- [53] H. Davoudiasl, P. B. Denton, and J. Gehrlein, Attractive scenario for light dark matter direct detection, Phys. Rev. D 102, 091701 (2020), arXiv:2007.04989 [hep-ph].
- [54] W. H. Press and S. A. Teukolsky, On formation of close binaries by two-body tidal capture., Astrophys. J. 213, 183 (1977).
- [55] A. C. Fabian, J. E. Pringle, and M. J. Rees, Tidal capture formation of binary systems and X-ray sources in globular clusters., MNRAS 172, 15 (1975).
- [56] P. Pani and A. Loeb, Tidal capture of a primordial black hole by a neutron star: implications for constraints on dark matter, Journal of Cosmology and Astroparticle Physics 2014 (06), 026.
- [57] C. Cutler and L. Lindblom, The Effect of Viscosity on Neutron Star Oscillations, Astrophys.J. 314, 234 (1987).
- [58] N. Andersson, Modelling the dynamics of superfluid neutron stars, Astrophys. Space Sci. 308, 395 (2007), arXiv:astro-ph/0610192.
- [59] E. Flowers and N. Itoh, Transport properties of dense matter., Astrophys. J. 206, 218 (1976).
- [60] E. Flowers and N. Itoh, Transport properties of dense matter. II., Astrophys. J. 230, 847

(1979).

- [61] W. DeRocco, M. Galanis, and R. Lasenby, Dark matter scattering in astrophysical media: collective effects (2022), arXiv:2201.05167 [hep-ph].
- [62] D. Page, J. M. Lattimer, M. Prakash, and A. W. Steiner, Minimal cooling of neutron stars: A New paradigm, Astrophys. J. Suppl. 155, 623 (2004), arXiv:astro-ph/0403657.
- [63] D. Yakovlev and C. Pethick, Neutron star cooling, Annual Review of Astronomy and Astrophysics 42, 169 (2004).
- [64] D. G. Yakovlev, K. P. Levenfish, and Y. A. Shibanov, Cooling neutron stars and superfluidity in their interiors, Phys. Usp. 42, 737 (1999), arXiv:astro-ph/9906456.
- [65] T. A. Wagner, S. Schlamminger, J. H. Gundlach, and E. G. Adelberger, Torsion-balance tests of the weak equivalence principle, Class. Quant. Grav. 29, 184002 (2012), arXiv:1207.2442 [gr-qc].
- [66] E. R. Siegel, M. Hertzberg, and J. Fry, Probing Dark Matter Substructure with Pulsar Timing, Mon. Not. Roy. Astron. Soc. 382, 879 (2007), arXiv:astro-ph/0702546.
- [67] N. Seto and A. Cooray, Searching for primordial black hole dark matter with pulsar timing arrays, Astrophys. J. Lett. 659, L33 (2007), arXiv:astro-ph/0702586.
- [68] H. A. Clark, G. F. Lewis, and P. Scott, Investigating dark matter substructure with pulsar timing I. Constraints on ultracompact minihaloes, Mon. Not. Roy. Astron. Soc. 456, 1394 (2016), [Erratum: Mon.Not.Roy.Astron.Soc. 464, 2468 (2017)], arXiv:1509.02938 [astro-ph.CO].
- [69] K. Schutz and A. Liu, Pulsar timing can constrain primordial black holes in the LIGO mass window, Phys. Rev. D 95, 023002 (2017), arXiv:1610.04234 [astro-ph.CO].
- [70] K. Kashiyama and M. Oguri, Detectability of Small-Scale Dark Matter Clumps with Pulsar Timing Arrays, (2018), arXiv:1801.07847 [astro-ph.CO].
- [71] J. A. Ellis, M. Vallisneri, S. R. Taylor, and P. T. Baker, ENTERPRISE: Enhanced Numerical Toolbox Enabling a Robust PulsaR Inference SuitE (2019), ascl:1912.015.
- [72] J. Ellis and R. van Haasteren, PTMCMCSampler: Parallel tempering MCMC sampler package written in Python (2019), ascl:1912.017.
- [73] Z. Arzoumanian, A. Brazier, S. Burke-Spolaor, S. J. Chamberlin, S. Chatterjee, B. Christy, J. M. Cordes, N. J. Cornish, K. Crowter, P. B. Demorest, and et al., The nanograv nine-year data set: Limits on the isotropic stochastic gravitational wave background, The Astrophysical

- Journal **821**, 13 (2016).
- [74] J. S. Hazboun, J. Simon, X. Siemens, and J. D. Romano, Model dependence of bayesian gravitational-wave background statistics for pulsar timing arrays, The Astrophysical Journal 905, L6 (2020).
- [75] B. Sun, Z. Cao, and L. Shao, Constraints on fifth forces through perihelion precession of planets, Physical Review D **100**, 10.1103/physrevd.100.084030 (2019).
- [76] L. Shao, N. Wex, and M. Kramer, Testing the universality of free fall towards dark matter with radio pulsars, Phys. Rev. Lett. **120**, 241104 (2018), arXiv:1805.08408 [gr-qc].
- [77] C. W. Stubbs, Experimental limits on any long range nongravitational interaction between dark matter and ordinary matter, Phys. Rev. Lett. **70**, 119 (1993).
- [78] J. F. Navarro, C. S. Frenk, and S. D. M. White, The Structure of cold dark matter halos, Astrophys. J. 462, 563 (1996), arXiv:astro-ph/9508025.
- [79] M. Cautun, A. Benitez-Llambay, A. J. Deason, C. S. Frenk, A. Fattahi, F. A. Gómez, R. J. J. Grand, K. A. Oman, J. F. Navarro, and C. M. Simpson, The Milky Way total mass profile as inferred from Gaia DR2, Mon. Not. Roy. Astron. Soc. 494, 4291 (2020), arXiv:1911.04557 [astro-ph.GA].
- [80] J. I. Read, The Local Dark Matter Density, J. Phys. G 41, 063101 (2014), arXiv:1404.1938
 [astro-ph.GA].
- [81] J. P. Gardner *et al.*, The James Webb Space Telescope, Space Sci. Rev. **123**, 485 (2006), arXiv:astro-ph/0606175.
- [82] A. Weltman *et al.*, Fundamental physics with the Square Kilometre Array, Publ. Astron. Soc. Austral. **37**, e002 (2020), arXiv:1810.02680 [astro-ph.CO].
- [83] J. Bramante, B. J. Kavanagh, and N. Raj, Scattering searches for dark matter in subhalos: Neutron stars, cosmic rays, and old rocks, Physical Review Letters 128, 10.1103/physrevlett.128.231801 (2022).
- [84] C. Kouvaris, WIMP Annihilation and Cooling of Neutron Stars, Phys. Rev. D 77, 023006 (2008), arXiv:0708.2362 [astro-ph].
- [85] G. Bertone and M. Fairbairn, Compact Stars as Dark Matter Probes, Phys. Rev. D 77, 043515 (2008), arXiv:0709.1485 [astro-ph].
- [86] C. Kouvaris and P. Tinyakov, Can Neutron stars constrain Dark Matter?, Phys. Rev. D 82, 063531 (2010), arXiv:1004.0586 [astro-ph.GA].

- [87] A. de Lavallaz and M. Fairbairn, Neutron Stars as Dark Matter Probes, Phys. Rev. D 81, 123521 (2010), arXiv:1004.0629 [astro-ph.GA].
- [88] J. Bramante, A. Delgado, and A. Martin, Multiscatter stellar capture of dark matter, Phys. Rev. D 96, 063002 (2017), arXiv:1703.04043 [hep-ph].
- [89] D. McKeen, M. Pospelov, and N. Raj, Cosmological and astrophysical probes of dark baryons, Phys. Rev. D 103, 115002 (2021), arXiv:2012.09865 [hep-ph].
- [90] M. Olivares, J. Saavedra, J. R. Villanueva, and C. Leiva, Motion of charged particles on the Reissner-Nordström (Anti)-de Sitter black holes, Mod. Phys. Lett. A 26, 2923 (2011), arXiv:1101.0748 [gr-qc].
- [91] A. A. Abdo, K. S. Wood, M. E. DeCesar, F. Gargano, F. Giordano, P. S. Ray, D. Parent, A. K. Harding, M. C. Miller, D. L. Wood, and M. T. Wolff, PSR J0007+7303 in the CTA1 Supernova Remnant: New Gamma-Ray Results from Two Years of Fermi Large Area Telescope Observations, Astrophys. J. 744, 146 (2012), arXiv:1107.4151 [astro-ph.HE].
- [92] A. Basu, B. Shaw, D. Antonopoulou, M. J. Keith, A. G. Lyne, M. B. Mickaliger, B. W. Stappers, P. Weltevrede, and C. A. Jordan, The jodrell bank glitch catalogue: 106 new rotational glitches in 70 pulsars, Monthly Notices of the Royal Astronomical Society 510, 4049 (2021).
- [93] M. A. Livingstone, S. M. Ransom, F. Camilo, V. M. Kaspi, A. G. Lyne, M. Kramer, and I. H. Stairs, X-ray and radio timing of the pulsar in 3C 58, The Astrophysical Journal 706, 1163 (2009).
- [94] C. M. Espinoza, D. Antonopoulou, B. W. Stappers, A. Watts, and A. G. Lyne, Neutron star glitches have a substantial minimum size, Monthly Notices of the Royal Astronomical Society 440, 2755 (2014).